

NASA/TM-2020-5006941



LS-DYNA[®] Water Ditching Simulation of a Fokker F28 Fellowship Aircraft

Karen E. Jackson
National Institute of Aerospace, Hampton, Virginia

Jacob B. Putnam
Langley Research Center, Hampton, Virginia

September 2020

NASA STI Program . . . in Profile

Since its founding, NASA has been dedicated to the advancement of aeronautics and space science. The NASA scientific and technical information (STI) program plays a key part in helping NASA maintain this important role.

The NASA STI program operates under the auspices of the Agency Chief Information Officer. It collects, organizes, provides for archiving, and disseminates NASA's STI. The NASA STI program provides access to the NTRS Registered and its public interface, the NASA Technical Reports Server, thus providing one of the largest collections of aeronautical and space science STI in the world. Results are published in both non-NASA channels and by NASA in the NASA STI Report Series, which includes the following report types:

- **TECHNICAL PUBLICATION.** Reports of completed research or a major significant phase of research that present the results of NASA Programs and include extensive data or theoretical analysis. Includes compilations of significant scientific and technical data and information deemed to be of continuing reference value. NASA counter-part of peer-reviewed formal professional papers but has less stringent limitations on manuscript length and extent of graphic presentations.
- **TECHNICAL MEMORANDUM.** Scientific and technical findings that are preliminary or of specialized interest, e.g., quick release reports, working papers, and bibliographies that contain minimal annotation. Does not contain extensive analysis.
- **CONTRACTOR REPORT.** Scientific and technical findings by NASA-sponsored contractors and grantees.

- **CONFERENCE PUBLICATION.** Collected papers from scientific and technical conferences, symposia, seminars, or other meetings sponsored or co-sponsored by NASA.
- **SPECIAL PUBLICATION.** Scientific, technical, or historical information from NASA programs, projects, and missions, often concerned with subjects having substantial public interest.
- **TECHNICAL TRANSLATION.** English-language translations of foreign scientific and technical material pertinent to NASA's mission.

Specialized services also include organizing and publishing research results, distributing specialized research announcements and feeds, providing information desk and personal search support, and enabling data exchange services.

For more information about the NASA STI program, see the following:

- Access the NASA STI program home page at <http://www.sti.nasa.gov>
- E-mail your question to help@sti.nasa.gov
- Phone the NASA STI Information Desk at 757-864-9658
- Write to:
NASA STI Information Desk
Mail Stop 148
NASA Langley Research Center
Hampton, VA 23681-2199

NASA/TM-2020-5006941



LS-DYNA[®] Water Ditching Simulation of a Fokker F28 Fellowship Aircraft

Karen E. Jackson
National Institute of Aerospace, Hampton, Virginia

Jacob B. Putnam
Langley Research Center, Hampton, Virginia

National Aeronautics and
Space Administration

Langley Research Center
Hampton, Virginia 23681-2199

September 2020

The use of trademarks or names of manufacturers in this report is for accurate reporting and does not constitute an official endorsement, either expressed or implied, of such products or manufacturers by the National Aeronautics and Space Administration.

Available from:

NASA STI Program / Mail Stop 148
NASA Langley Research Center
Hampton, VA 23681-2199
Fax: 757-864-6500

TABLE OF CONTENTS

	Page No.
1. ABSTRACT	1
2. INTRODUCTION	1
3. DEVELOPMENT OF THE F28 WATER IMPACT MODEL	6
4. RESULTS	8
4.1 A320 Recovery and Damage Assessment	8
4.2 F28 Predicted Structural Responses	10
4.2.1 Seat Base Responses	10
4.2.2 Airframe Responses	15
4.3 F28 Predicted Kinematic Responses, Impact Sequences, and Damage	17
4.3.1 Kinematic Responses	17
4.3.2 Impact Sequences	17
4.3.3 Damage	21
4.4 F28 Predicted Occupant Responses and Injury Risk Assessment	24
5. DISCUSSION OF RESULTS	32
6. CONCLUSIONS	34
7. REFERENCES	35

LIST OF FIGURES

	Page No.
1. Post-impact photographs of the US Airways A320 depicting passenger egress.	2
2. Photographs of the Fokker F28 and the Airbus A320.	4
3. Full-scale crash test of a Fokker F28 aircraft.	5
4. Final LS-DYNA® model of the F28 aircraft impacting soft soil.	5
5. F28 water impact model with void.	6
6. Top, side, and front views of the F28 model and water block, but without void.	7
7. Montage of photographs of the A320 aircraft being recovered.	9
8. Photographs showing damage to the A320 aircraft following recovery.	10
9. Side view comparisons of model and actual deformation and damage.	10
10. Schematic of the F28 aircraft showing the locations of seat base accelerometers.	11
11. Representation of the seat/occupant masses.	11
12. Forward acceleration responses of the seat bases of Rows 2, 6, and 11 on the Port side.	12
13. Vertical acceleration responses of the seat bases of Row 2, 6, and 11 on the Port side.	13
14. Forward acceleration responses of the seat bases of Rows 2, 6, and 12 on the Starboard side.	14
15. Vertical acceleration responses of the seat bases of Row 2, 6, and 12 on the Starboard side.	14
16. Photograph of an airframe accelerometer, that was used in the 2019 crash test of the F28.	15
17. Forward and vertical acceleration responses of airframe locations in the forward cabin, mid-cabin and aft cabin locations on the Port side.	16
18. Forward and vertical acceleration responses of airframe locations in the forward cabin, mid-cabin and aft cabin locations on the Starboard side.	16
19. Forward (left) and vertical (right) velocity responses of the F28 model.	17
20. Side view impact sequence.	20
21. Isometric impact sequence.	21
22. Damage sequence.	23
23. Schematic of position and configuration of ATDs simulated.	24
24. Occupant breakout models.	25
25. Normalized injury metric responses predicted in the front section of the aircraft (top) and reference schematic of ATD positioning (bottom)	28
26. Row 3 Starboard ATD kinematic response at completion of simulation: FAA H3 50 th versus THOR	29
27. Row 6 Port ATD kinematics: braced vs nominal position.	29
28. Row 5 Port ATD kinematics (top) and upper neck response time history (bottom): H3 5 th vs H3 95 th .	30
29. Normalized injury metric responses predicted in the wing-box section of the Aircraft (top) and reference schematic of ATD positioning (bottom)	31

LIST OF FIGURES (Completed)

- | | |
|---|----|
| 30. Normalized injury metric responses predicted in the Aft section of the aircraft (top),
reference schematic of ATD positioning (bottom-left), and seat support deformation
observed in simulation of seat 10C (bottom-right) | 32 |
| 31. Mesh distortion. | 34 |

LIST OF TABLES

Table No.	Title	Page No.
1.	Comparisons of the Fokker F28 and the Airbus A320 Aircraft	4
2.	Number of Total Failed Elements per Timestep	22
3.	Computed Injury Metric Responses	27

LIST OF ACRONYMS

Acronym	Definition
AAR	Aircraft Accident Report
A320	Airbus transport aircraft
ALE	Arbitrary Lagrangian-Eulerian
ATD	Anthropomorphic Test Devise
CG	Center-of-Gravity
CNRB	Constrained Nodal Rigid Body
EFG	Element Free Galerkin
F28	Fokker Fellowship aircraft
FAA	Federal Aviation Administration
FE	Finite Element
FS	Fuselage Station
FSI	Fluid-Structure Interaction
ft	foot
g	acceleration of gravity
H3	Hybrid III
HIC	Head Injury Criteria
Hz	Hertz
IAA	Inter-Agency Agreement
ICFD	Incompressible Computational Fluid Dynamics
in	inch
ISO	International Organization of Standards
LandIR	Landing and Impact Research
lb	pound
NACA	National Advisory Committee on Aeronautics
NASA	National Aeronautics and Space Administration
NHTSA	National Highway Traffic Safety Administration
NTSB	National Transportation Safety Board
Nij	Neck Injury Criteria
s	second
SMP	Symmetric Multi-Processing
SPH	Smoothed Particle Hydrodynamics
THOR	Test device for Human Occupant Restraint
TR	Technical Report
US	United States

LS-DYNA® Water Ditching Simulation of a Fokker F28 Fellowship Aircraft

Karen E. Jackson
Senior Research Engineer
National Institute of Aerospace

Jacob B. Putnam
Research Engineer
NASA Langley Research Center

1. ABSTRACT

A previously validated finite element model of a Fokker F28 Fellowship aircraft was used to perform LS-DYNA® simulations for water ditching conditions consistent with US Airways Flight 1549 crash into the Hudson River. The LS-DYNA® model of the F28 was originally developed from an existing NASTRAN loads model and was validated through test-analysis comparisons with data from a full-scale crash test of the F28 onto soil. The F28 aircraft was simulated for the Flight 1549 impact conditions, not to precisely predict the response of the Airbus A320 aircraft used for that flight, but to evaluate tools for simulating and analyzing water impacts using a realistic aircraft ditching event. Flight 1549 impact conditions were: V_x (forward velocity) = 211 ft/s (2,532 in/s) and V_z (vertical velocity) = 12.5 ft/s (150 in/s). The impact attitude was: Roll = 0.0°, Pitch (nose up) = 9.5°, and Yaw = 0.0°. This Fluid-Structure Interaction simulation was executed using the Arbitrary Lagrangian-Eulerian capability in LS-DYNA®. Results are presented in several categories: F28 predicted structural (seat base and airframe) accelerations; F28 predicted model kinematic responses, impact sequences, and damage; and F28 predicted occupant responses and injury risk assessment. Findings of the simulation show that predicted seat base and airframe accelerations in both the vertical and forward directions were relatively low, approximately 15 g or less, resulting in a fairly benign impact event. Likewise, simulations of the occupant breakout models predicted injury risk values well below the defined safety limits for dynamic loading certification. The F28 simulation had similar aft fuselage damage and a low probability of passenger injury consistent with the actual US Airways Flight 1549 ditching event.

2. INTRODUCTION

On January 15, 2009, a US Airways Airbus A320 transport aircraft crashed under controlled impact conditions into the Hudson River in New York City after hitting a flock of birds, which caused failure of its two engines. The plane carried 150 passengers and 5 crew members, all of whom survived the impact, egressed the aircraft successfully, and were rescued by river ferries and the Coast Guard (see Figure 1). Flight 1549 took off from LaGuardia Airport and was on its way to Charlotte, North Carolina when the bird strike occurred, shortly after take-off. One news report of the incident stated that "...successful emergency landing in water is among the rarest and most dangerous feats in commercial flying [1]." This statement is confirmed by accident statistics for transport aircraft experiencing water impact, as reported in Reference 2.

The A320 incident represents a controlled crash into water under nearly ideal conditions and provides an opportunity to evaluate the real-world effects of water impact on a transport category airplane. There is a question as to whether this incident should be classified as a water ditching or a crash into water. The ditching certification criterion is based on a 1957 National Advisory Committee on Aeronautics (NACA) report that documents scale-model testing in a 2,900 ft long tow tank [3]. Ditching is an emergency landing in water. For an official "ditching" to occur, certain impact parameters must be present. For example, the descent rate cannot be greater than 5 ft/s, and the longitudinal and vertical loads must be within aircraft design parameters, as described in Reference 2. The National Transportation Safety Board (NTSB) in their Aircraft Accident Report (AAR-10/03, Reference 4) states: "The NTSB considers this accident to be a ditching because the pilots clearly intended to ditch on the Hudson River. The accident falls between a planned and unplanned event in that, although the pilots did not have time to complete each step of the applicable checklist, they did have sufficient time to consult the Quick Reference Handbook, begin checklist execution, transmit radio calls, determine a landing strategy, configure the airplane for ditching, and alert the flight attendants and passengers to "brace for impact" [4].



(a) Side view photo of Flight 1549 showing passenger egress.



(b) Front view photograph of Flight 1549 showing passenger egress.

Figure 1. Post-impact photographs of the US Airways A320 depicting passenger egress.

Based on this discussion, the Flight 1549 incident could be designated a ditching, even though the impact conditions were higher than those specified for ditching. The velocity of the aircraft at the moment of impact was determined by the NTSB to be V_x (forward velocity) = 211 ft/s (2,532 in/s)

and V_z (vertical velocity) = 12.5 ft/s (150 in/s). The impact attitude was: Roll = 0.0°, Pitch (nose-up) = 9.5°, and Yaw = 0.0°. A detailed and documented assessment of structural damage was made following recovery of the airframe. This accident provides a unique opportunity to develop water impact models, to simulate airframe and occupant responses, and to compare analytical predictions with kinematic and occupant responses from the water impact event. Additional information on the NTSB investigation is documented in Reference 4.

Commercial nonlinear transient dynamic finite element codes, such as LS-DYNA® [5], are capable of simulating problems involving Fluid-Structure Interaction (FSI) using a variety of solvers including Arbitrary Lagrangian-Eulerian (ALE), Smoothed Particle Hydrodynamics (SPH), Element Free Galerkin (EFG), and Incompressible Computational Fluid Dynamics (ICFD). Using the ALE formulation, the aircraft structure is modeled using a purely Lagrangian mesh composed of deformable elements with associated nodes that move with the element. The fluid, or water, is typically modeled using a stationary Eulerian mesh in which the fluid material flows, while conserving mass, momentum, and energy. When using the ALE algorithm, a portion of the volume above the water must also be modeled with an Eulerian mesh to allow wave formation and fluid movement, thus enabling prediction of the water splash at impact. The advantage of ALE is that an accurate physical representation of fluid behavior is possible while also allowing prediction of the nonlinear progressive damage to the structural model. It should be noted that the approach of using the ALE water mesh and the fluid-structure coupling algorithm in LS-DYNA® has been validated for Orion and other water impact studies [6-10]. The accuracy of the methodology is dependent on mesh discretization; however, the F28 water ditching simulation utilized the calibrated parameters that define the ALE mesh and the coupling algorithm from these earlier studies.

A previously validated finite element model of a Fokker F28 Fellowship aircraft was used to simulate the impact conditions of the US Airways Flight 1549 ditching event. Although replicating the ditching conditions is the focus of this analysis, there are significant differences which should be noted between the aircraft in the event, an Airbus A320, and the Fokker F28 aircraft simulated. Photographs of these two aircraft are shown, side-by-side, in Figure 2. A comparison of structural details of these two aircraft is listed in Table 1.

The Fokker F28 is roughly half the size of an Airbus A320 and has less than half of the total weight. In addition, the engine nacelles in the F28 are located above the wing, while the engine nacelles in the A320 are located below the wing. However, despite these differences, a finite element model of the Fokker F28 was simulated using the impact conditions of US Airways Flight 1549 ditching event, as the goal of this analysis was to simulate the ditching conditions, and not to predict the actual A320 response.



(a) Fokker F28.

(b) Airbus A320.

Figure 2. Photographs of the Fokker F28 and the Airbus A320.

Table 1. Comparisons of the Fokker F28 and the Airbus A320 Aircraft

Parameter	Fokker F28	Airbus A320
Classification	Regional Jet	Jet Airliner
Length, ft.	89	123
Wingspan, ft.	77	117
Weight, lb.	35,517 (empty)	82,100
Range, nmiles	920	3,300
Seating Capacity, passengers	65	150-186
Number of Crew	5	6

In 2000, a retired Fokker F28 Fellowship aircraft, along with two sets of wings and three fuselage sections (two forward sections and a wing-box section), were obtained during the NASA Aviation Safety Program [11]. The F28 is a high-performance twin-turbofan narrow-body aircraft with seating in a 3+2 configuration. The F28 was first type certified by the FAA in 1969 and the F28 fleet has since been retired from service in the United States. A photograph of the aircraft arriving at Langley field is shown in Figure 2(a). Following arrival, all useful interior structures and equipment including avionics and other electronics, seats, and hat racks were removed. All fuel lines were drained, and the engines were also removed. An Inter-Agency Agreement (IAA) was signed between the National Aeronautics and Space Administration (NASA) Langley Research Center and the Federal Aviation Administration (FAA) in September 2016, to create a cooperative research effort to obtain data through a series of tests that support the development of airframe level crash requirements for transport category airplanes [12].

Under the IAA, vertical drop tests and LS-DYNA[®] simulations of two F28 fuselage sections were conducted at NASA Langley. The results of this test-analysis effort are documented in References 13-17. The test program culminated in June 2019 with a full-scale crash test of the Fokker F28 aircraft that was conducted at the Landing and Impact Research (LandIR) Facility at NASA Langley [18]. The test article weighed 33,306 lb and impacted a 2 ft high soil bed. Pre- and post-

test photographs of the crash test are shown in Figure 3. As documented in Reference 19, the primary damage to the airframe consisted of skin wrinkling and buckling, and failure of the Port side wing attachments. In the interior of the aircraft, the rear floor buckled, though the seats remained attached to the seat rails.

As mentioned previously, a finite element model of the F28 aircraft was created from an existing NASTRAN [20] loads model, which was obtained from Fokker at the same time that the hardware was purchased. Considerable work was expended to convert the model into a viable representation of the aircraft and into LS-DYNA® format. This work included changing the system of units, adding elements to represent missing structures, and defining and reconnecting the mesh. The final model of the June 2019 crash test is depicted in Figure 4. The model contained representations of the soil bed, the airframe, the rigid wall placed at the end of the soil bed to prevent the airframe from sliding into the Hydro Impact Basin at LandIR, and two drag chains that were added to help slow the aircraft down after impact.

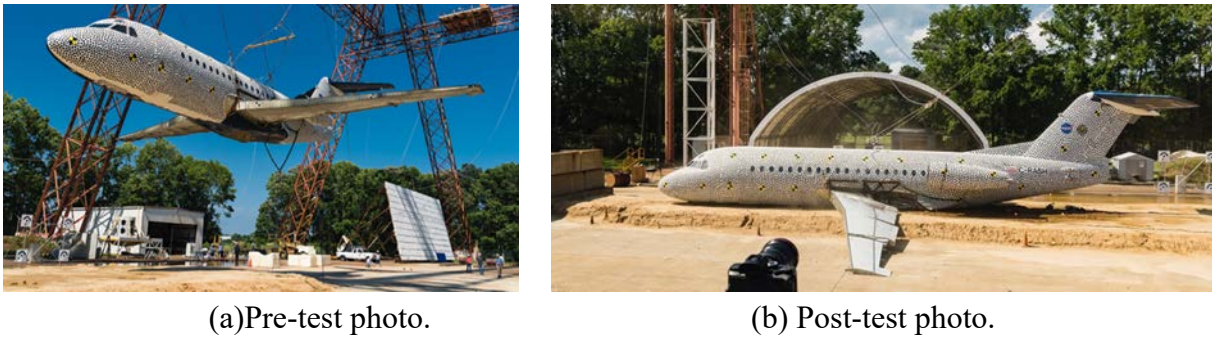


Figure 3. Full-scale crash test of a Fokker F28 aircraft.

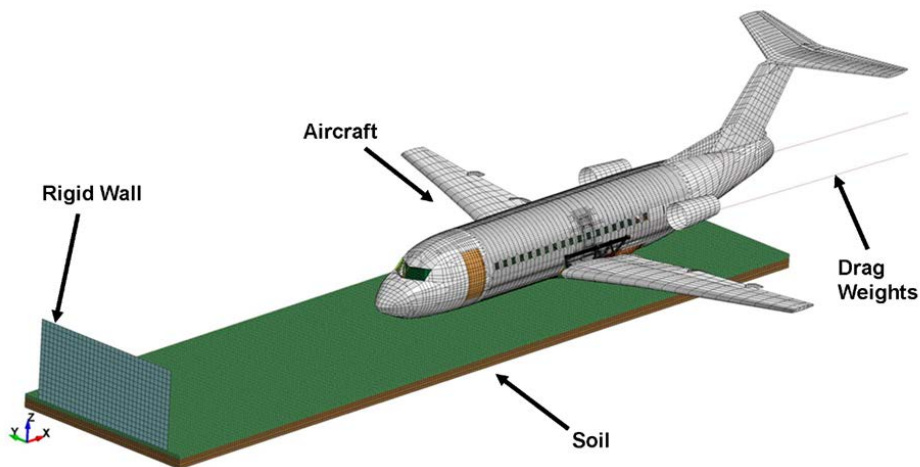


Figure 4. Final LS-DYNA® model of the F28 aircraft impacting soft soil.

Test-analysis comparisons of the F28 impact into soil are documented in References 21 and 22. These results are presented in several categories: inertial property comparisons; kinematic

comparisons; structural acceleration comparisons; airframe deformation and failure; occupant responses; and, quantitative test-analysis correlation results. The inertial properties, such as total weight and Center-of-Gravity (CG) location were predicted within 6.6%. Kinematic comparisons show close prediction of forward and vertical velocities of the vehicle throughout impact. Total slide-out distance was predicted to within 1.4%. Structural acceleration comparisons focused on data from accelerometers located at the seat bases, the airframes, and four discrete locations. As a means of quantifying test-analysis results, the International Organization of Standards (ISO) Technical Report (ISO/TR-16250) curve comparison methodology was used [23]. Using this methodology 61 of the 67 test-analysis responses (91%) were deemed accurate [21]. Based on these findings, the F28 finite element model is considered validated for the land landing condition evaluated.

This paper will document simulations of a LS-DYNA® finite element model of the F28 aircraft impacting water under conditions that match US Airways Flight 1549, which crashed into the Hudson River following engine failures caused by bird strikes. The paper will describe: (1) Development of the F28 water impact model; (2) A320 recovery and damage assessment, (3) F28 predicted structural accelerations, (4) F28 predicted kinematic responses, impact sequences, and damage, and (5) F28 predicted occupant responses and injury risk assessment.

3. DEVELOPMENT OF THE F28 WATER IMPACT MODEL

Several changes were made to the F28 finite element model, shown in Figure 4, so that it could be used for the water ditching simulation. The drag chain, soil, and rigid wall were removed. Several openings on the surface of the model were closed, such that the exterior surface of the aircraft was watertight. In addition, shell elements composing the outer mold line of the vehicle were adjusted so that the normal direction of each element faced outwards. A large block of solid elements was added to create the water, which is located just beneath the bottom of the aircraft. Another block was added above the water to represent the void. For simplification, the void was assigned *MAT_NULL material properties. Coupling and contact of the Lagrangian and Eulerian meshes to solve the FSI problem are accomplished by using the *CONSTRAINED_LAGRANGE_IN_SOLID command in LS-DYNA®. A side view of the model is shown in Figure 5, in which the void is represented as a transparent block.

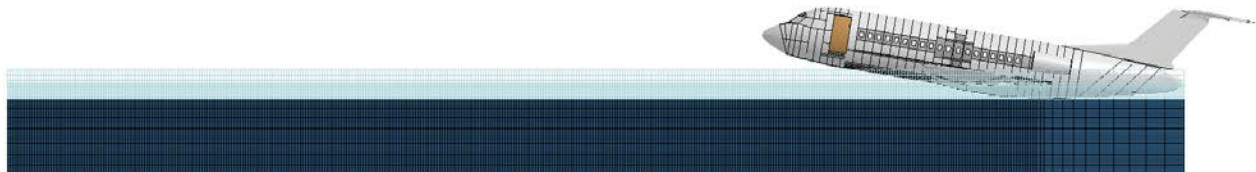
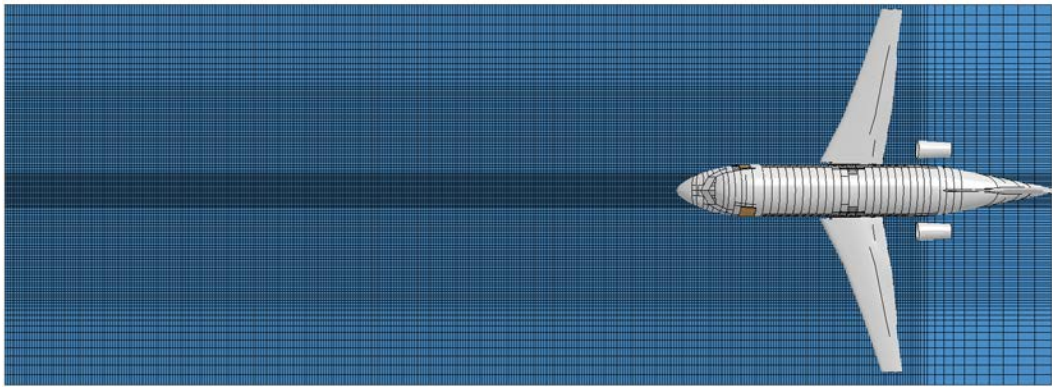


Figure 5. F28 water impact model with void.

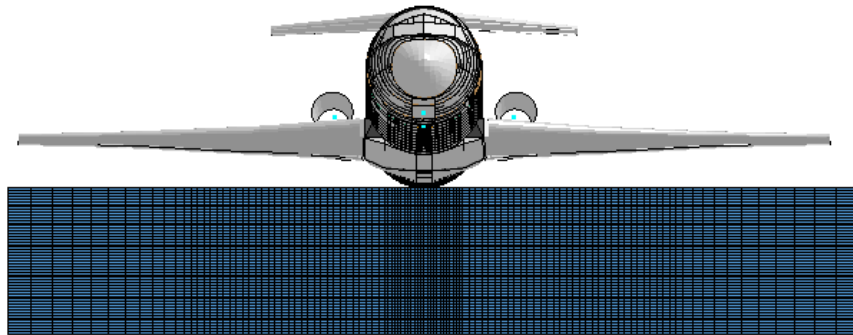
The model is depicted in Figure 6, without the void, in three orthogonal directions. As shown in both Figures 5 and 6, the aircraft model is pitched nose-up by 9.5° to match the actual attitude of the A320 as it hit the Hudson River. The aircraft model contained: 745 parts; 75 material cards; 1,299,220 nodes; 26,026 beam elements; 81,093 shell elements; 19,682 solid elements; 34 element masses; and, 76 Constrained Nodal Rigid Bodies (CNRBs). The water and void blocks were 164 ft x 80 ft x 12 ft (Length x Width x Height) and the mesh was refined along the primary impact path, as shown in Figure 6(a). Together, the water and void blocks were created using an additional 1,808,882 solid elements. The aircraft model was assigned initial velocity conditions to match those found in the NTSB report [4], which were V_x (forward velocity) = 211 ft/s (2,532 in/s) and V_z (vertical velocity) = 12.5 ft/s (150 in/s). Note that the vertical impact velocity is relatively small compared with previously conducted drop tests. For example, the F28 fuselage section drop tests were performed at 28.9 ft/s (346.8 in/s) for the forward section and 29.1 ft/s (349.2 in/s) for the wing-box section, as described in Reference 14.



(a) Top view.



(b) Side view.



(c) Front view.

Figure 6. Top, side, and front views of the F28 model and water block, but without void.

The model was executed using LS-DYNA® Symmetric Multi-Processing (SMP) version R11.1.0 (double precision) on 8 processors of a Linux-based workstation computer and required 1,902 hours (79.25 days) of clock time to reach normal termination of 1.0 seconds. The reason for the exceptionally long runtime was that the parameter ‘nadv’ on the *CONTROL_ALE card was set to 1, which required that the mesh be advected every timestep. As stated in Reference 24, “Eulerian and ALE (Arbitrary Lagrangian-Eulerian) hydrodynamics programs usually split a timestep into two parts. The first part is a Lagrangian step, which calculates the incremental motion of the material. The second part is referred to as the Eulerian step, the advection step, or the remap step, and it accounts for the transport of material between cells. In most finite difference and finite element formulations, all of the solution variables, except the velocities, are cell-centered while the velocities are edge- or vertex-centered. As a result, the advection algorithm for the momentum is, by necessity, different than the algorithm used for the other variables.” Typically, in an ALE finite element simulation, advection techniques are used to stabilize the mesh.

4. RESULTS

Results are presented in several categories including: A320 Recovery and Damage Assessment; F28 Predicted Structural Responses; F28 Predicted Kinematic Responses, Impact Sequences, and Damage; and F28 Predicted Occupant Responses and Injury Risk Assessment.

4.1 A320 Recovery and Damage Assessment

Two weeks after the initial water impact, on January 23, 2009, the NTSB initiated recovery of the aircraft. The A320 aircraft had sunk approximately 50 ft to the bottom of the Hudson River. A large barge with a heavy crane was moved to the impact site. A loading frame was constructed to raise the aircraft from beneath both wing attachment locations. Photographs of the recovery effort are shown in Figure 7. It is interesting to note that the recovery started at approximately 5:30 PM and was completed at 1:30 AM the next morning, or 8 hours later. The reason for the long duration was an attempt to reduce the possibility that additional damage to the aircraft might be incurred during recovery as it was raised through the water.

Post-recovery photographs of damage to the aircraft are shown in Figure 8. Most of the damage occurred in the tail section, which impacted the water first given the 9.5° pitch attitude of the aircraft. As shown in Figure 8(c), many of the damaged parts were removed, providing a “clean” view of the tail section. The A320 aircraft is now located in the Carolinas Aviation Museum in Charlotte, North Carolina.

Damage to the F28 aircraft model, which was simulated for the same impact conditions as US Airways Flight 1549, is depicted in Figure 9(a). In addition, a side view of the A320 aircraft is shown for comparison in Figure 9(b). As stated previously, most of the damage was located in the rear of the aircraft and in the tail section. Unfortunately, even with the long recovery time, it is

not possible to separate the damage that occurred during the crash event from any potential damage produced during recovery of the aircraft.

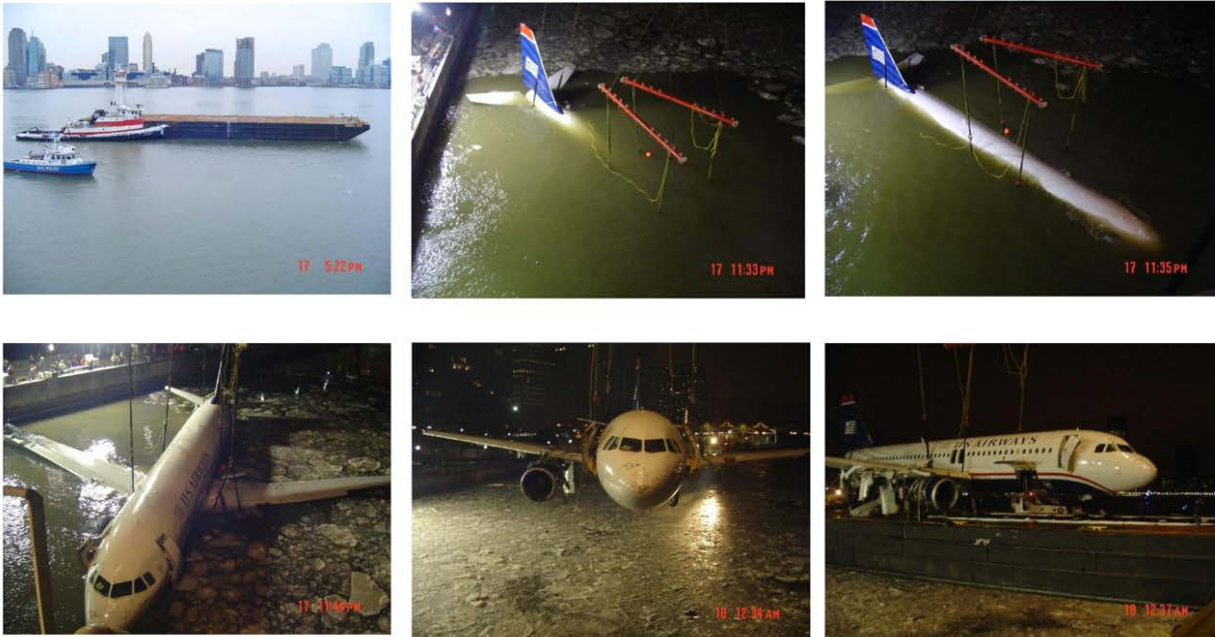


Figure 7. Montage of photographs of the A320 aircraft being recovered.



Damage to the tail section, looking forward.

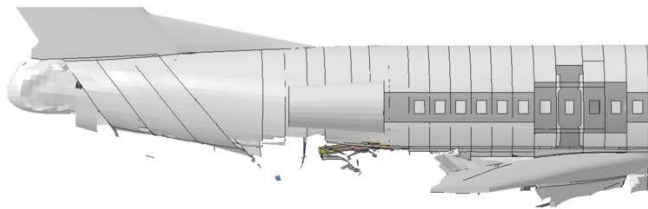


(b) Damage to the tail section, looking aft.



(c) Tail section of the A320 after removal of damaged parts.

Figure 8. Photographs showing damage to the A320 aircraft following recovery.



(a) F28 model deformation.



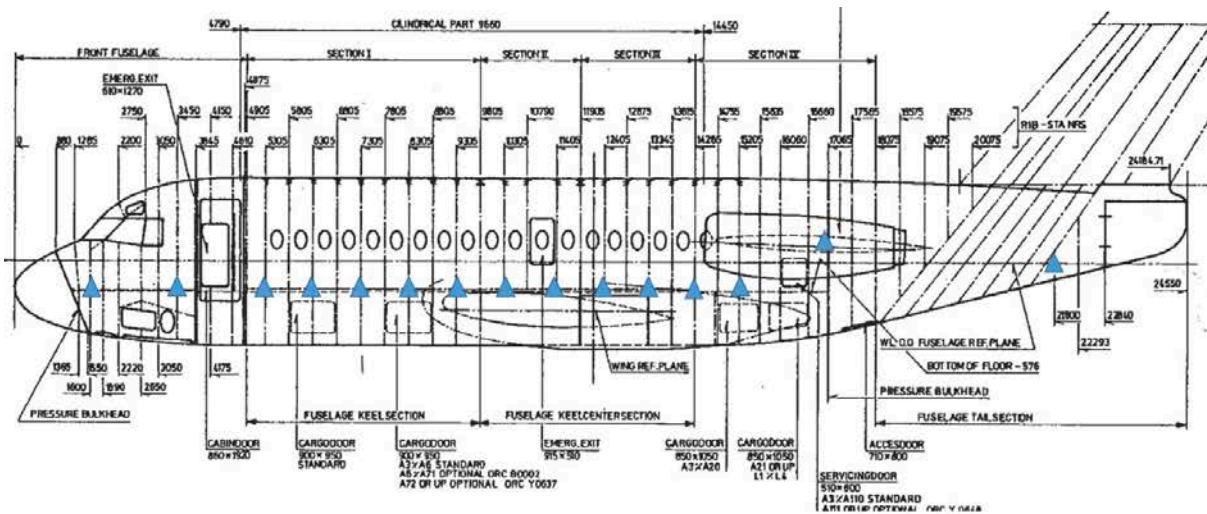
(b) Photograph of A320 aircraft damage.

Figure 9. Side view comparisons of F28 model and actual A320 damage.

4.2 F28 Predicted Structural Responses

4.2.1 Seat Base Responses

Time history responses were obtained from seat bases at several locations in the F28 airframe, fore and aft. These locations are depicted as blue triangles in Figure 10(a). A photograph of a typical seat base accelerometer that was used in the 2019 F28 crash test onto soil is shown in Figure 10(b). Note that the seats and occupants were represented in the model as concentrated masses that were placed at the approximate CG location of the seat/occupant. CNRBs were used to attach the concentrated masses to the floor at the location of the seat base. A depiction of the seat/occupant masses is shown in Figure 11. Finally, note that all acceleration time histories presented herein were filtered using a low-pass 50 Hz 4-pole Butterworth filter. Also, local coordinate systems were defined at each nodal location for output of acceleration responses.



(a) Schematic of the F28 aircraft showing the locations of seat base/floor accelerometers.



(b) Photo of a typical seat base accelerometer used in the 2019 crash test of the F28 onto soil.

Figure 10. Schematic of the F28 aircraft showing the location of a seat base accelerometer and a photo of an actual seat base accelerometer.

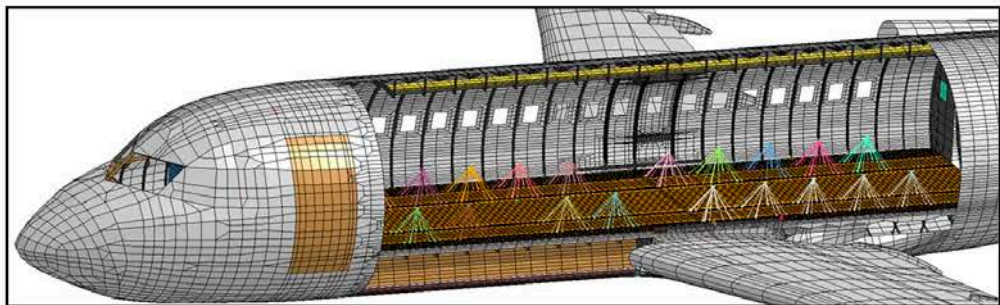
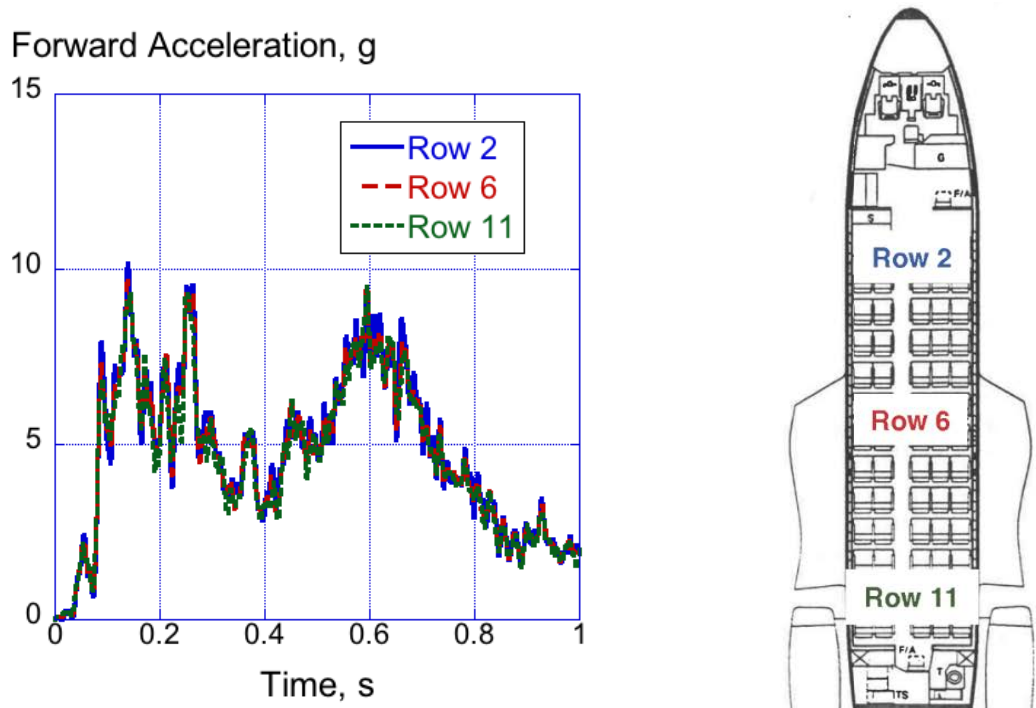


Figure 11. Representation of the seat/occupant masses.

The initial time history responses examined were the forward acceleration responses of the seat bases of Row 2 (forward cabin), Row 6 (mid-cabin), and Row 11 (aft cabin) which are plotted for

the Port side in Figure 12(a). Note that these seat locations are shown schematically in Figure 12(b). The forward acceleration responses are nearly identical and do not show any differences across the length of the aircraft. Note that the magnitudes of the forward acceleration responses are low. Except for one peak, all forward acceleration responses are less than 10 g.



(a) Forward acceleration plot.

(b) Schematic showing the seat locations.

Figure 12. Forward acceleration responses of the seat bases of Rows 2, 6, and 11 on the Port side.

The vertical acceleration responses are plotted in Figure 13(a) for seat bases at Row 2, Row 6, and Row 11 on the Port side of the aircraft. Even with 50 Hz filtering, these traces contain highly oscillatory vibrations. For the first 0.3 s of the pulse, the response of the seat base at Row 11 shows the highest magnitude peaks, likely due to the initial impact of the aircraft, which may induce the oscillatory response. The acceleration response of the seat base at Row 2, which is located in the forward cabin, exhibits three peaks of 11 g, 8 g, and 6.5 g from 0.4 s to the end of the pulse. It is speculated that the 11 g spike in the vertical acceleration response of the Row 2 seat base that occurs just after 0.4 s, may be attributed to slap down of the aircraft. Slap down occurs following initial tail strike, as the aircraft rotates about its CG until the nose section impacts the water at a higher velocity than the initial impact. Finally, note that the overall magnitude of the responses is generally low, less than 15 g. In an attempt to clarify the vertical acceleration responses, the traces were replotted with filtering at 20 Hz in Figure 13(b).

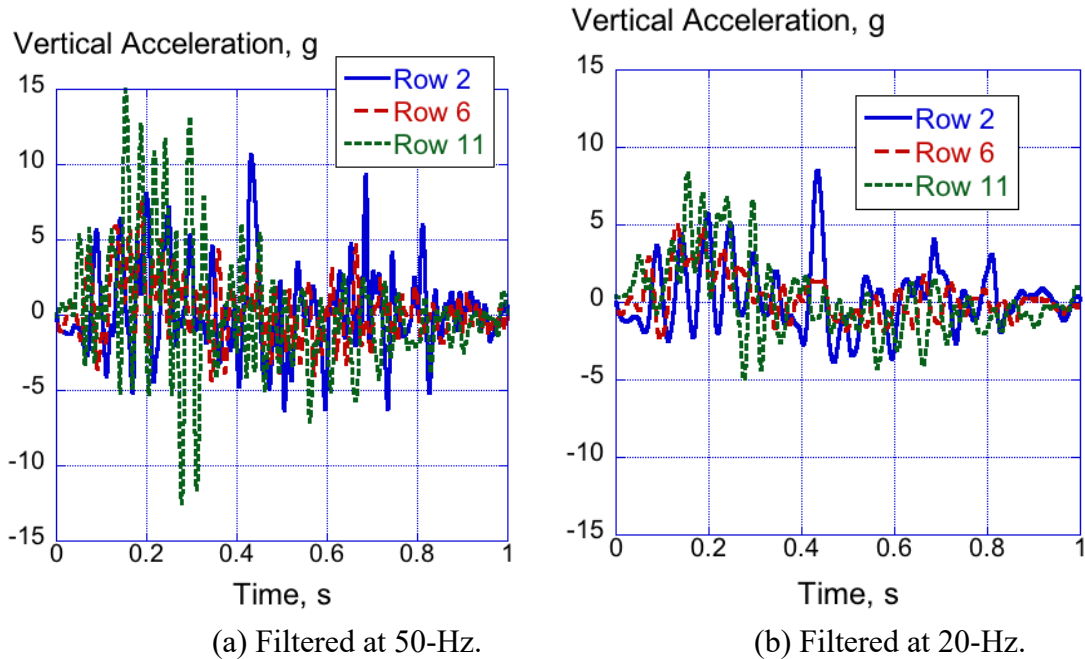
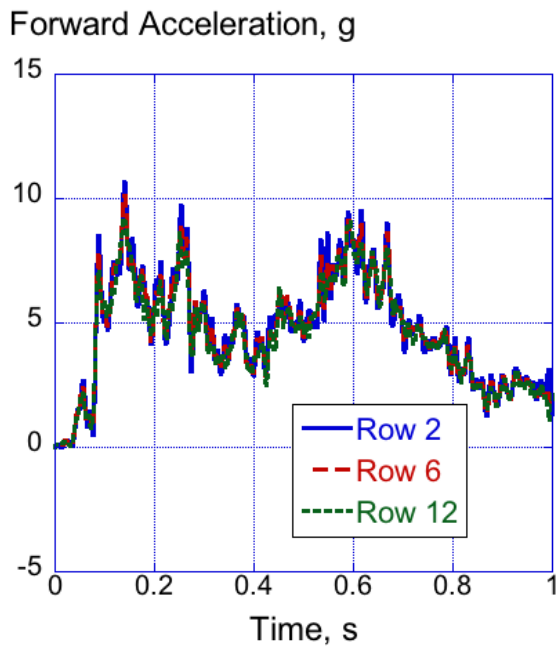


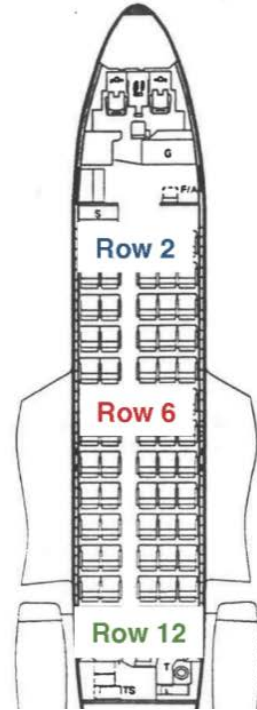
Figure 13. Vertical acceleration responses of the seat bases of Row 2, 6, and 11 on the Port side.

The forward acceleration responses of the seat bases of Row 2 (forward cabin), Row 6 (mid-cabin), and Row 12 (aft cabin) are plotted for the Starboard side in Figure 14(a). Note that these seat locations are shown schematically in Figure 14(b). Once again, the three acceleration curves are practically identical. Almost no difference is seen between the Port and Starboard forward acceleration responses. With the exception of one peak, the magnitudes of all forward acceleration responses are less than 10-g.

Finally, the vertical acceleration responses are plotted in Figure 15(a) for seat bases at Row 2, Row 6, and Row 12 on the Starboard side of the aircraft. Once again, the acceleration time histories contain highly oscillatory vibrations, even after filtering. As was seen for the Port side, the aft response (Row 12) exhibits the highest magnitude peaks during the early portion of the pulse. By 0.4 seconds, the forward seat base position (Row 2) exhibits the highest magnitude peak of 12.5 g. In an attempt to clarify the vertical acceleration responses, the traces were replotted with filtering at 20 Hz in Figure 15(b). Once again, the overall magnitudes of these responses are low, less than 15 g. As noted for the Port side vertical acceleration responses, the 12.5 g peak in the Row 2 seat base may be attributed to aircraft slap down.

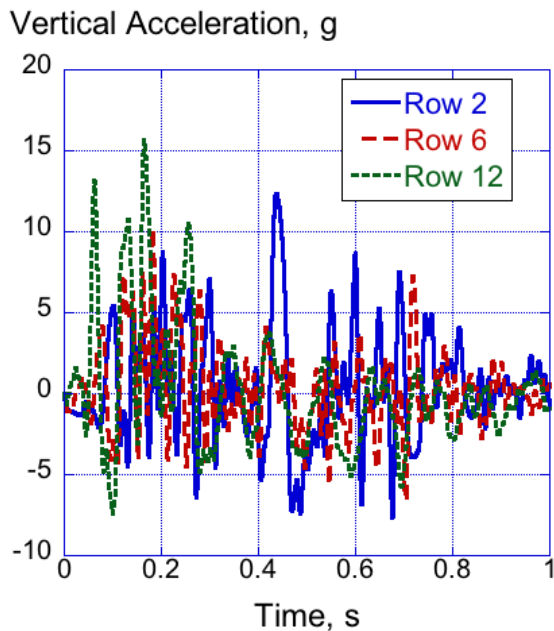


(a) Forward acceleration plot.

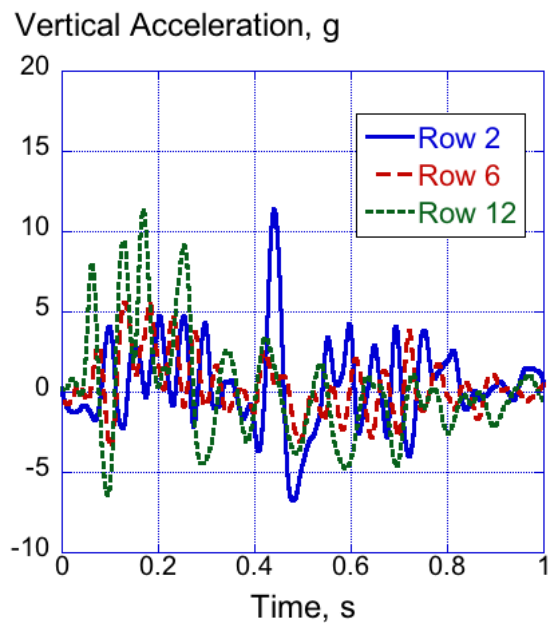


(b) Schematic showing the seat locations.

Figure 14. Forward acceleration responses of the seat bases of Rows 2, 6, and 12 on the Starboard side.



(a) Filtered at 50-Hz.



(b) Filtered at 20-Hz.

Figure 15. Vertical acceleration responses of the seat bases of Row 2, 6, and 12 on the Starboard side.

4.2.2 F28 Predicted Airframe Responses

This section of the paper focuses on the predicted airframe responses. A photograph is shown in Figure 16, which shows the location of a typical airframe accelerometer in the F28 crash test article. The accelerometer is located on the airframe web, approximately 2 in. above the floor. Please note that all acceleration responses output from the model were generated using a local coordinate system.



Figure 16. Photo of an airframe accelerometer, that was used in the 2019 crash test of the F28.

The Port side forward and vertical acceleration responses are shown in Figures 17(a) and (b), respectively, for three airframe locations: one at a forward Fuselage Station (FS), one at a mid-cabin FS, and one at an aft cabin FS location. The three forward acceleration responses, shown in Figure 17(a), have nearly identical shapes, magnitudes, and durations with little or no difference due to longitudinal position. The vertical acceleration responses, however, are different. Even after filtering using a low-pass filter with a cutoff frequency of 50 Hz, the three responses contain high frequency vibrations. It is interesting to note that the aft vertical response exhibits the highest peaks early in the pulse, to about 0.3 s, after which time, the forward FS response has the highest magnitude peaks for the remainder of the pulse. Note that no slap down effect is evident in the forward FS airframe response. Still, the magnitudes of the forward and vertical acceleration responses are low, less than 15 g, except for one peak.

The Starboard side forward and vertical acceleration responses are shown in Figure 18(a) and (b), respectively, for three airframe locations: one forward FS, one mid-cabin FS, and one aft cabin FS location. The three forward acceleration responses, shown in Figure 18(a), have nearly identical shapes, magnitudes, and durations with little or no difference based on longitudinal position. These curves are also similar to the forward acceleration responses on the Port side, as shown in Figure 17(a). Once again, the overall magnitude of the forward acceleration responses is low, less than 10 g. Even after filtering using a low-pass filter with a cutoff frequency of 50 Hz, the three

vertical airframe responses contain high frequency vibrations. It is interesting to note that the aft FS vertical response exhibits the highest peaks early in the pulse; however, the forward FS vertical response exhibits the highest peaks in the later portion of the pulse. As noted previously, the Starboard airframe acceleration responses are low in magnitude, less than 20 g.

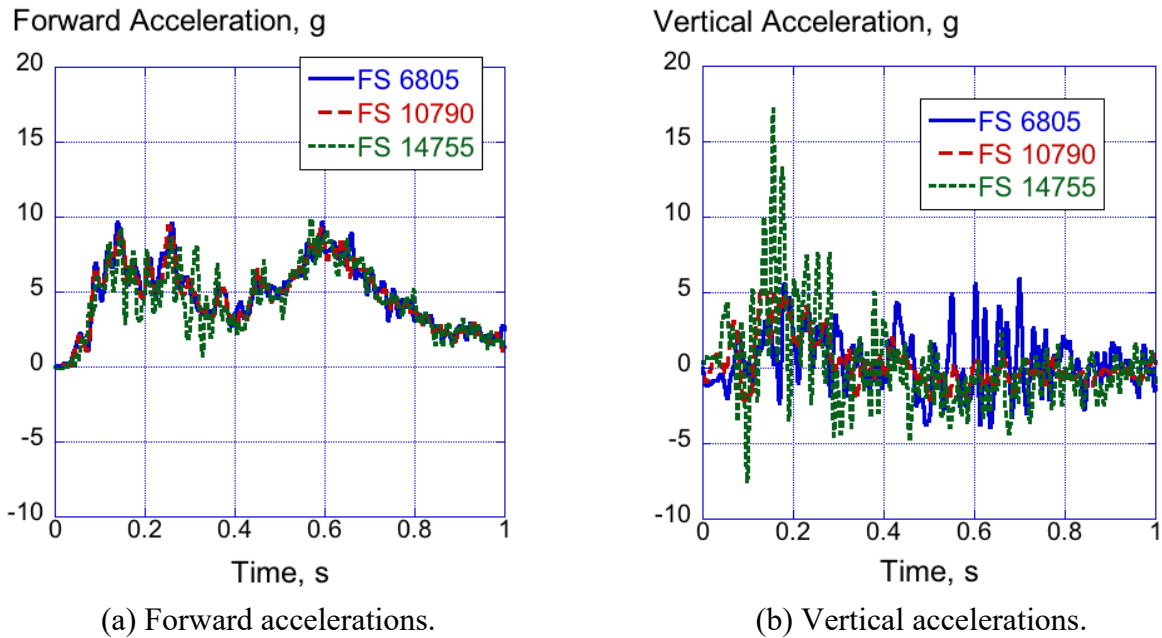


Figure 17. Forward and vertical acceleration responses of airframe locations on the Port side.

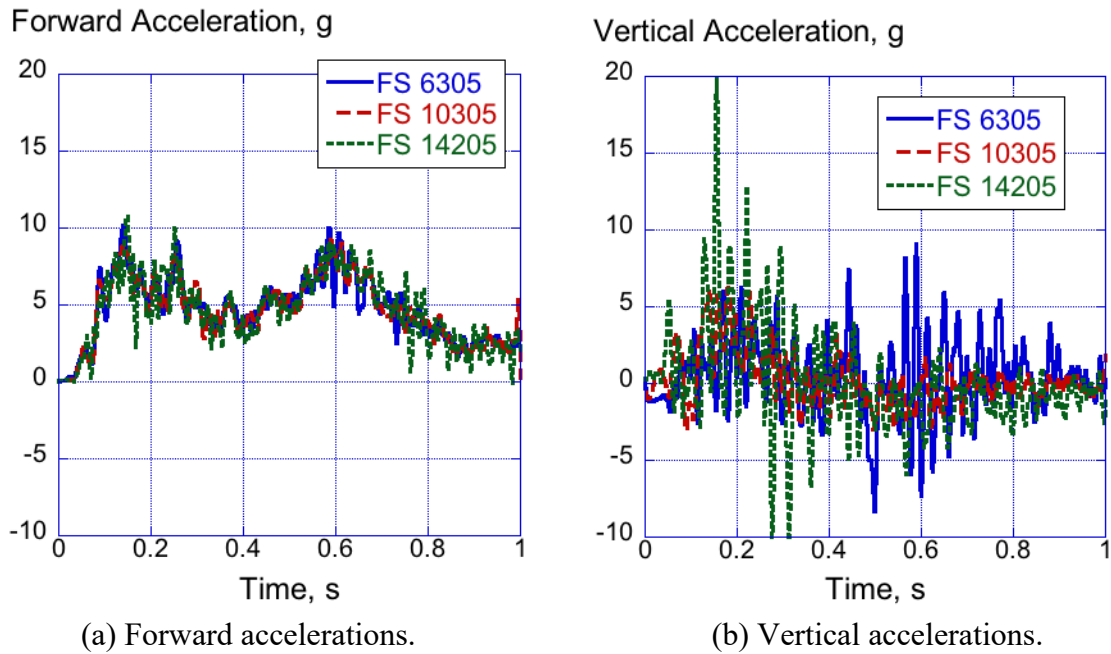


Figure 18. Forward and vertical acceleration responses of airframe locations on the Starboard side.

4.3 F28 Predicted Kinematic Responses, Impact Sequences, and Damage

4.3.1 Kinematic Responses

Kinematic responses focus on the gross motion of the model as impact occurs including the timing of events, contact with the impact surface, and subsequent slide-out. For this assessment, plots of forward and vertical velocity were determined by selecting several nodes, at random, on the sides and along the top of the aircraft model. Altogether, nine different nodes were selected. The velocity responses were obtained for each node and averaged to generate the plots, shown in Figure 19. These unfiltered plots were created directly from the LS-DYNA[®] binary output files and were not generated by integration of acceleration responses. Several points can be made, based on the data shown in Figure 19. First, even though the model was executed for 1.0 second duration, the forward velocity has not crossed zero and the model has approximately 700 in/s of residual forward velocity. In contrast, the vertical velocity response indicates that the model has crossed zero velocity at 0.435 s, rebounded to a maximum of 21 in/s, and is well on its way to crossing zero again by the end of the pulse. Note that the initial vertical velocity of 150 in/s was considerably smaller than the initial forward velocity of 2,532 in/s.

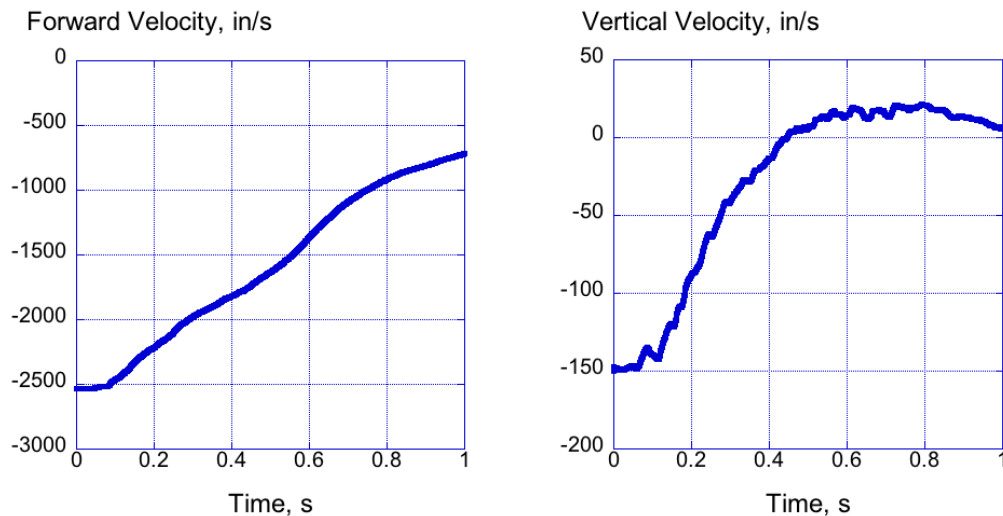











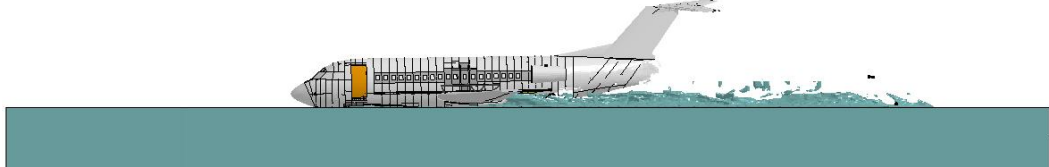
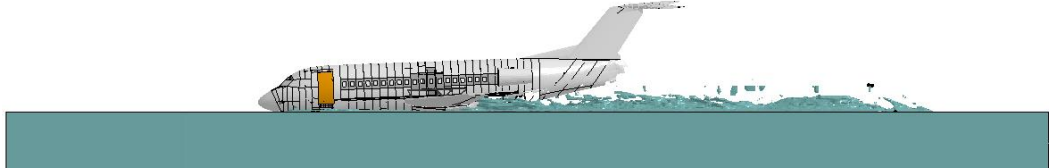


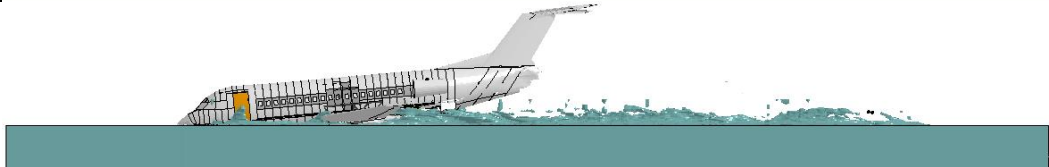
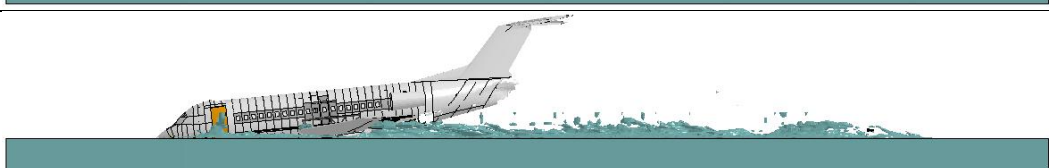
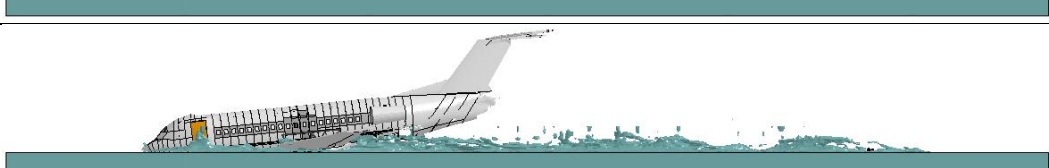
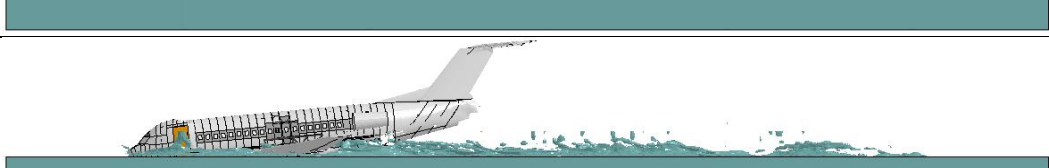
Figure 19. Forward (left) and vertical (Right) velocity responses of the F28 model.

4.3.2 Impact Sequences

Two impact sequences are shown in Figures 20 and 21. Figure 20 shows a side view of the impact sequence for 21 time steps, from 0.0 to 1.0 s in 0.05 s increments. This impact sequence shows the wave action as the aircraft impacts the water, as well as the progressive damage to the aircraft, which is located near the rear cargo hold and the tail. The initial pitch attitude (nose-up) of the aircraft disappears by 0.4 seconds, as the aircraft rotates to become level. After this time, the nose of the aircraft appears to “dig” into the water slightly, as the tail of the aircraft rises. The second impact sequence, shown in Figure 21, shows an isometric view of the aircraft for 10 time steps,

from 0.1 to 1.0 seconds in 0.1 second increments. This view of the impact sequence shows less damage to the aircraft and more water deformation and wave formation.

Time, s	Side view of Model
0.00	
0.05	
0.1	
0.15	
0.2	
0.25	
0.3	
0.35	
0.4	

0.45	
0.5	
0.55	
0.6	
0.65	
0.7	
0.75	
0.8	

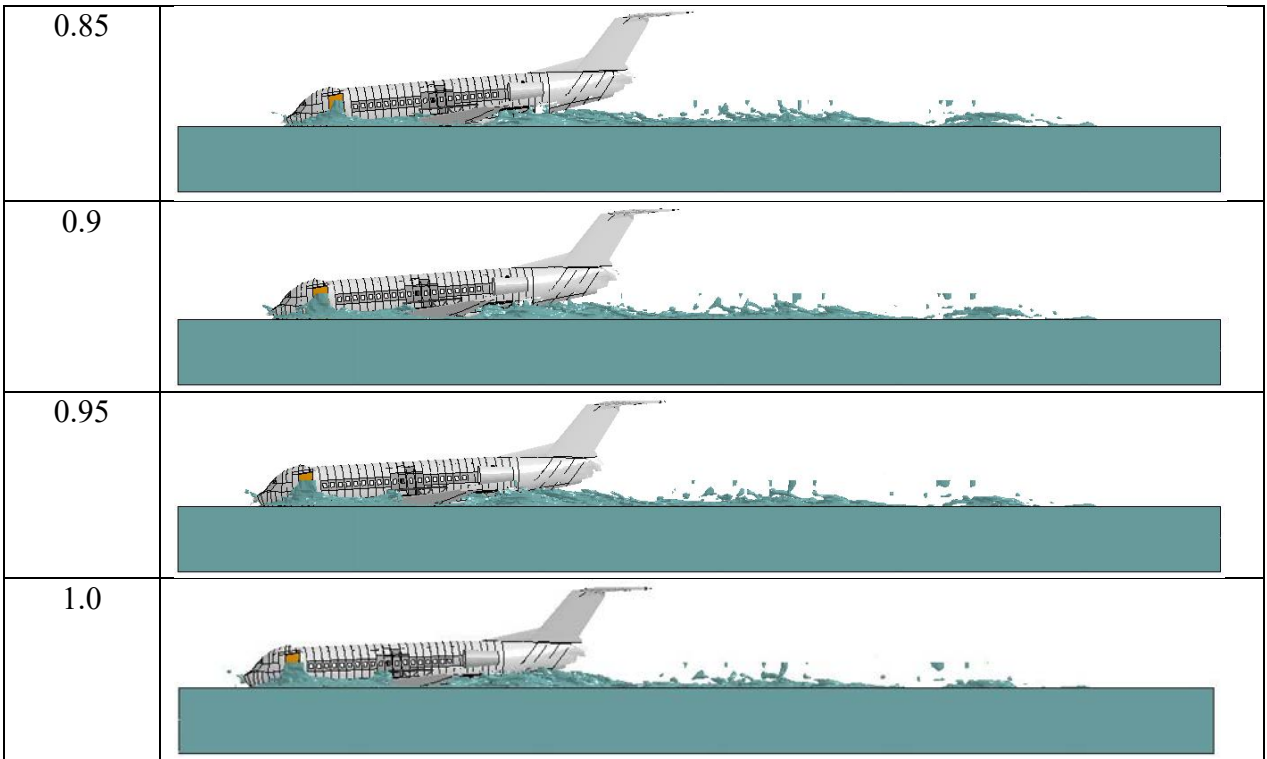
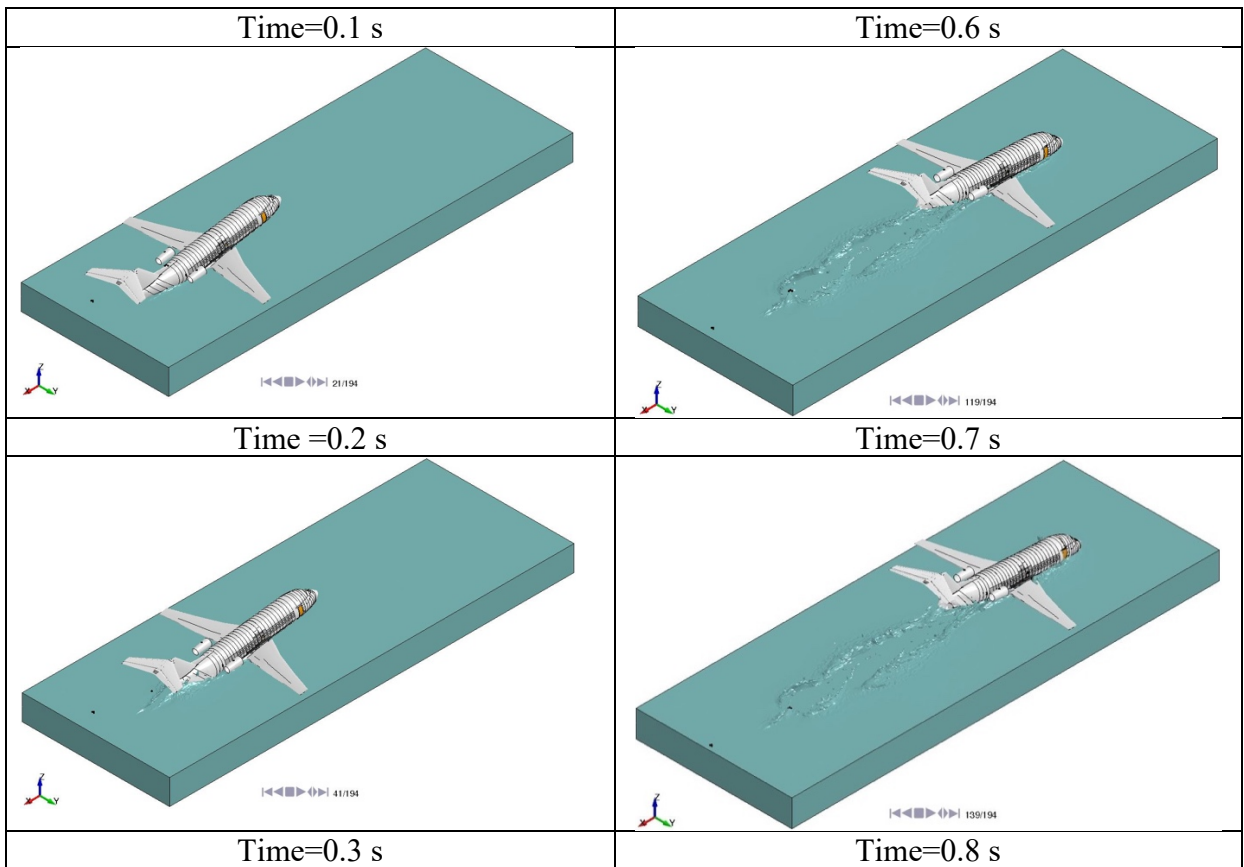


Figure 20. Side view impact sequence.



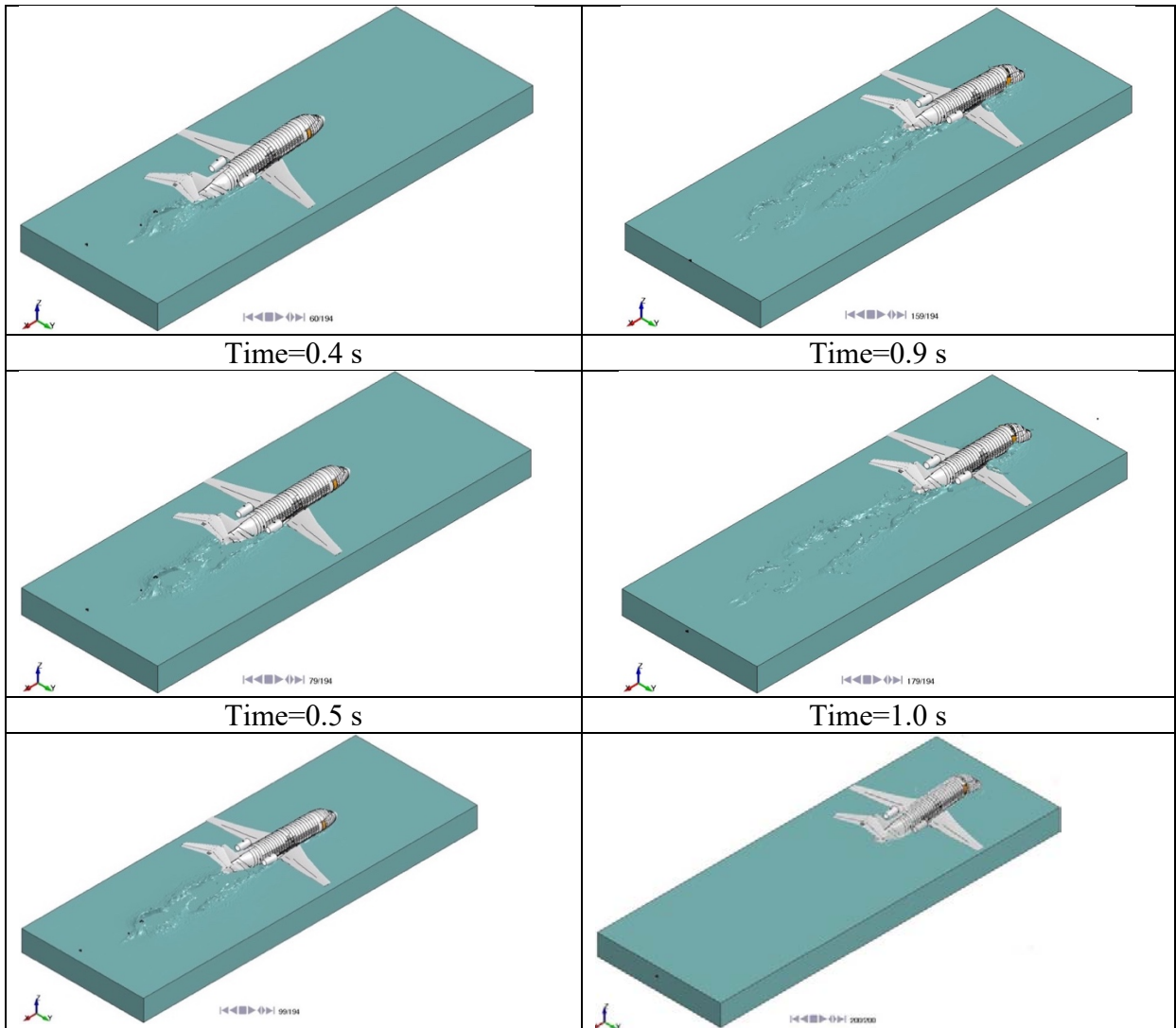


Figure 21. Isometric impact sequence.

4.3.3 Damage

As the rear portion of the outer skin and tail structure impact the water, elements in that region of the aircraft model begin to deform under pressure loading. These elements are assigned elastic-plastic material properties with a failure strain. Once the stress level exceeds the yield limit of the material, then the elements begin to exhibit plastic deformation. At an average effective plastic strain limit of 0.15, the elements will fail or erode. Both terms have the same meaning, which is that the “failed” element is removed from the simulation. In general, failed elements are undesirable in explicit finite element simulations in that removed elements create holes in the mesh, which can initiate instability. However, in the present simulation, elements were allowed to fail.

Table 2 lists the total number of failed beam, shell, and solid elements in the model for each time step from 0.0 to 1.0 s in 0.05 s increments. In addition, the table lists the number of failed elements

that have increased from the previous time step. For example, the number of failed elements at 0.1 s is 326. The previous time step (0.05 s) had 35 failed elements. Consequently, the number of increased failed elements is $326 - 35 = 291$. The data shown in Table 2 indicate that damage primarily occurs in two time phases, initially between 0.15 and 0.25 s and again between 0.6 to 0.8 s. Note that the forward acceleration responses of the seat bases and airframe locations on both the Port and Starboard sides, shown in Figures 12(a), 14(a), 17(a), and 18(a), exhibit two peaks that match the same two time phases.

As a final assessment of aircraft damage, an impact sequence of a portion of the aircraft located in the lower rear fuselage aft of the wing is shown in Figure 22. This sequence shows that by 0.2 s, most of the outer skin has failed, thus exposing the support structure for the floor. Fortunately, the floor structure did not fail, and the water did not intrude into the cabin during the impact sequence. Note that a side view of the aircraft is shown in Figure 9(a), which illustrates the overall magnitude of the damage to the lower rear section of the aircraft.

Table 2. Number of Total Failed Elements per Timestep

Time, s	Total No. of Failed Elements	Number Increased
0.0	0	0
0.05	35	35
0.1	326	291
0.15	838	512
0.2	1248	410
0.25	1528	280
0.3	1737	209
0.35	1831	94
0.4	1893	62
0.45	1967	74
0.5	2095	128
0.55	2321	226
0.6	2661	340
0.65	3161	500
0.7	3563	402
0.75	3769	206
0.8	3917	148
0.85	4019	102
0.9	4069	50
0.95	4112	43
1.0	4132	20

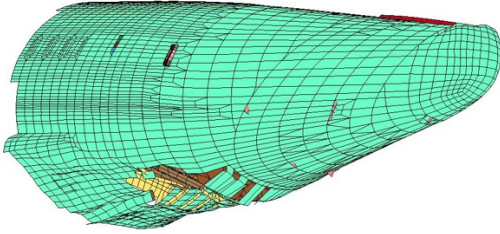
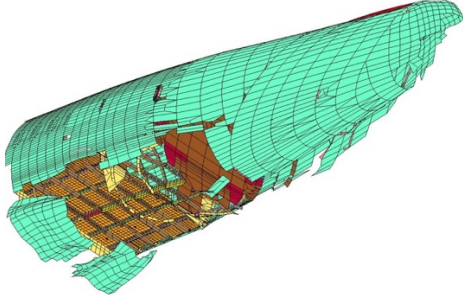
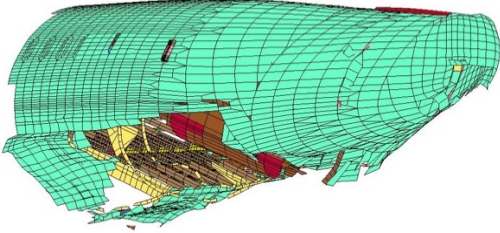
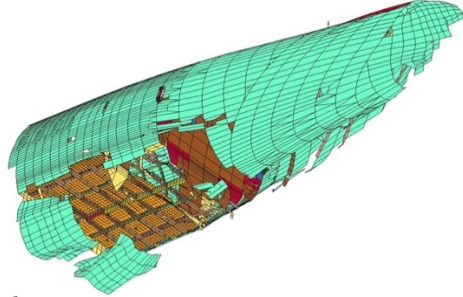
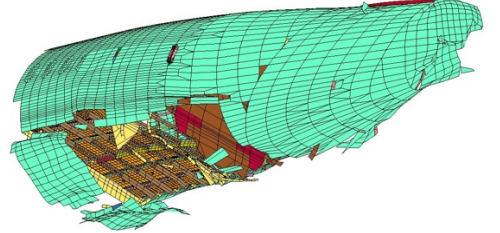
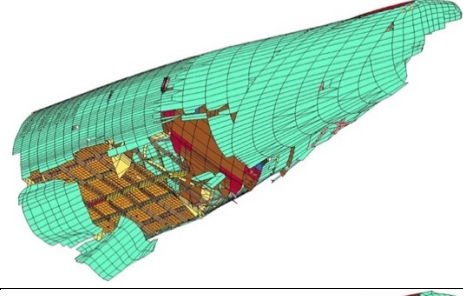
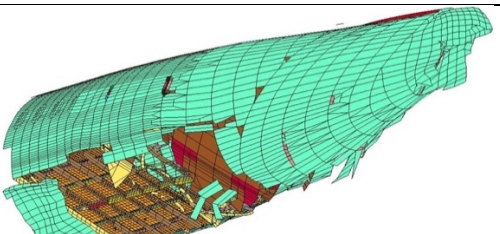
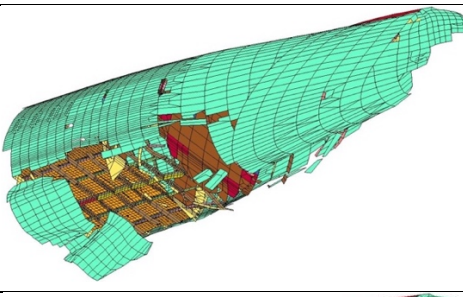
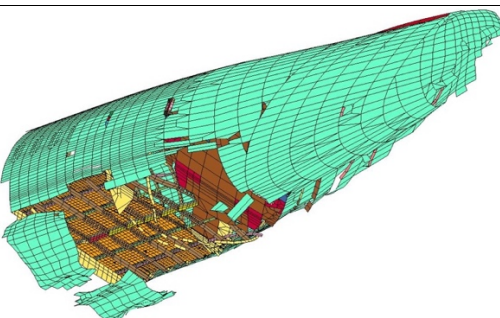
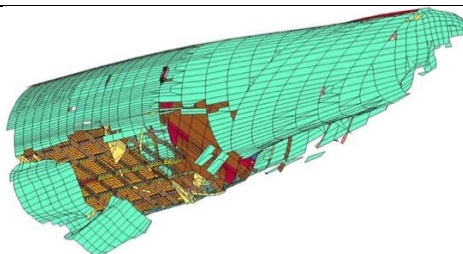
Depiction of Lower Rear Fuselage Damage			
Time, s		Time, s	
0.1		0.6	
0.2		0.7	
0.3		0.8	
0.4		0.9	
0.5		1.0	

Figure 22. Damage sequence.

4.4 F28 Predicted Occupant Responses and Injury Risk Assessment

To evaluate occupant responses for the Fokker F28 aircraft simulated under the Flight 1549 ditching event conditions, occupant models were developed for each of the seating locations previously evaluated in the F28 land landing test and simulation [22]. Occupants were represented by a variety of Anthropomorphic Test Device (ATD) finite element (FE) models:

- (1) Humanetics® Hybrid III FAA 50th percentile version 1.2.3 (H3 FAA 50th) [25],
- (2) Humanetics® Hybrid III 5th percentile version 7.0.5 (H3 5th) [26],
- (3) LSTC® Hybrid III 95th percentile beta version 3.03 (H3 95th) [27], and
- (4) Test device for Human Occupant Restraint (THOR) version 2.1 publicly released by the National Highway Traffic Safety Administration (NHTSA) with modifications made by NASA to improve accuracy under vertical loading [28-30].

The distribution of simulated occupants throughout the aircraft is provided in Figure 23.

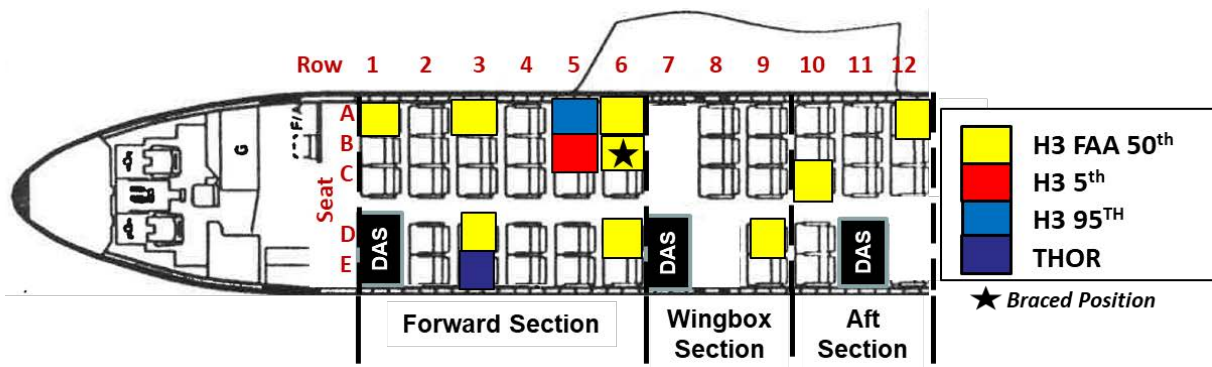


Figure 23. Schematic of position and configuration of ATDs simulated.

For each seating group, an individual occupant breakout model was created. The occupant breakout model was made up of the seated ATD model, a representative belt model, and all attached seats, as well as the forward row of seats with which the ATD may interact during the impact event. Nine occupant breakout models were simulated, made up of five Starboard and four Port side seat rows (see Figure 24). Nine FAA H3 50th, one H3 5th, one H3 95th, and one THOR ATD model were simulated. The ATD models were positioned within the seats to match the conditions tested in the 2019 Fokker F28 land landing crash test. This arrangement included one FAA H3 50th in the braced position in seat 6D. Two occupant breakout models did not include a forward seat, Row 1 Starboard and Row 9 Port. This condition matched the previously tested configuration [Ref. 21] and was roughly representative of a bulkhead and exit door seats. The development of these occupant breakout models, including seat and belt model generation as well as ATD positioning is described in full detail in Reference 22.

To simulate each occupant breakout model in the crash event, the linear acceleration and rotational velocity predicted at the seat base accelerometer locations that were generated by the F28 ditching simulation were applied to the occupant breakout models at nodes matching the accelerometer

locations. This loading condition was applied locally as it was measured in the full-vehicle simulation. To drive seat motion, the node was rigidly fixed to the seat at the seat-to-floor attachment location. The occupant breakout simulations were performed for 0.3 seconds, which encompassed peak acceleration input from the vehicle impact, as well as completion of the contact event with the forward seatback in applicable seating configurations. All simulations were performed on a Linux computer cluster using LS-DYNA® [31] SMP Version R10.1.0 double precision with four processors. Simulation runtimes ranged from 26 to 106 hours depending on the quantity and variant of ATDs in the occupant breakout model.

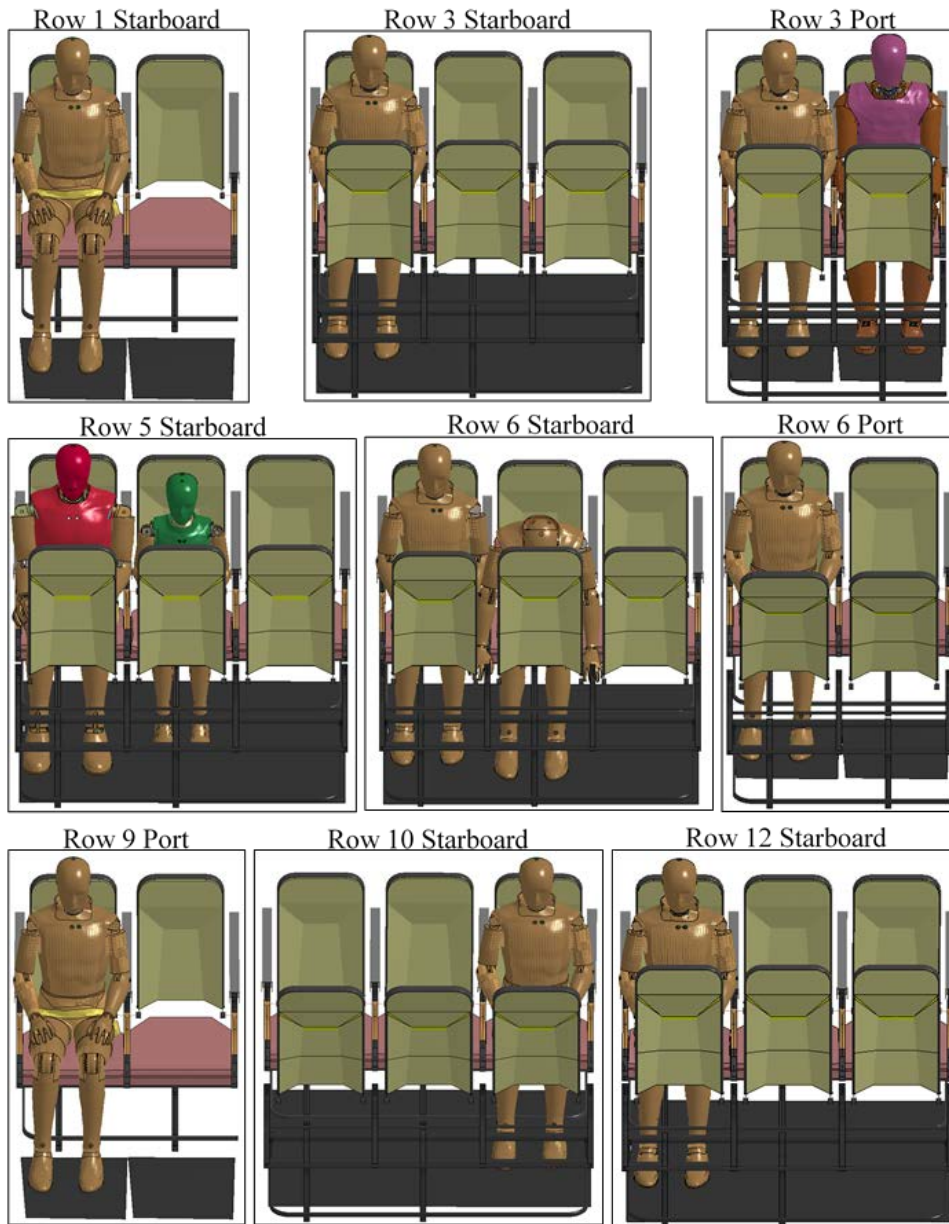


Figure 24. Occupant breakout models.

Occupant responses in the F28 ditching simulation were quantified through four different injury metrics: Head Injury Criteria (HIC-15), HIC-36, Neck Injury Criteria (Nij), and lumbar load. The HIC and lumbar load injury metrics are currently defined by the FAA for certification of occupant safety under dynamic loading conditions [32]. Nij requirements are not defined by the FAA but are instead established as a requirement for automotive occupant safety defined by NHTSA [33]. Although not directly defined for aircraft certification, the Nij metric provides applicable assessment of neck injury that is not quantified by the HIC and lumbar load metrics. Each metric provides insight into occupant risk for different injury mechanisms potentially induced during a crash event. HIC quantifies head injury risk, namely skull fracture risk, and is primarily driven by any contact between the occupant head and the surrounding environment. Nij quantifies injury risk to the cervical spine due to flexion-extension and tension-compression of the neck during impact. This risk is induced through both inertial loading of the head-neck as well as contact loading of the head into the neck. The lumbar load criteria quantify injury risk to the lumbar spine, namely vertebral fracture, due to spinal compression. This risk is primarily induced through vertical acceleration experienced during impact being transferred through the seat and into the pelvis of the occupant causing compression of the spine into the upper body mass. HIC and lumbar load injury metrics were calculated for all simulated ATDs. Appropriate responses were compared to the limits defined for the FAA Hybrid III 50th ATD as FAA certification requirements for these metrics currently exist only for this ATD configuration [31]. The Nij metric calculation was made for each ATD configuration according to the certification standards defined by NHTSA [33, 34].

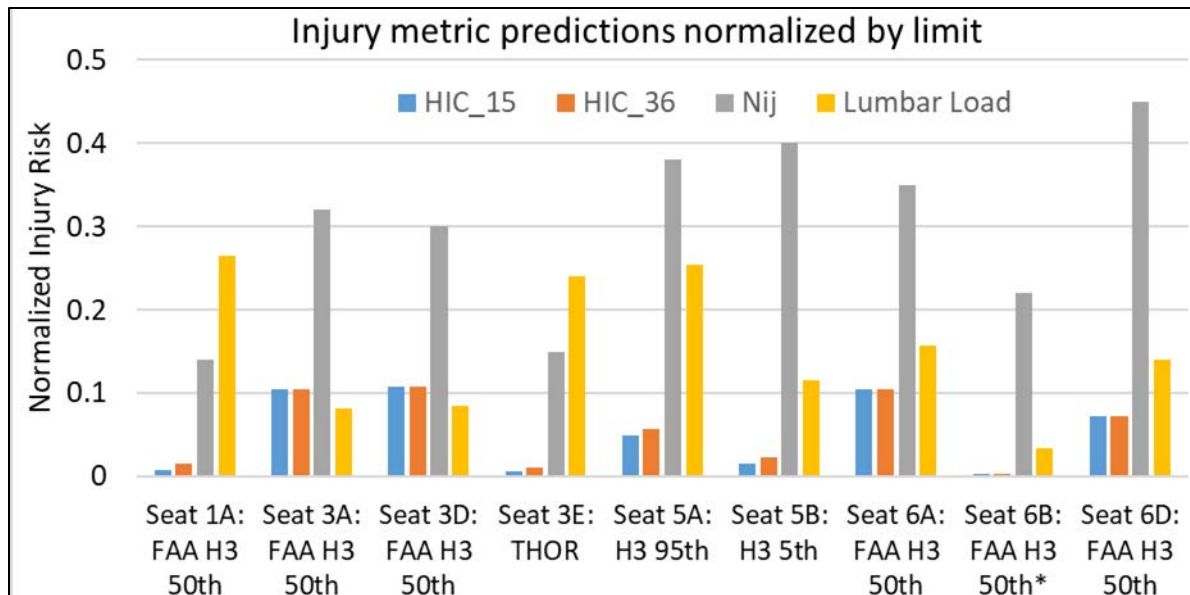
Simulation of the occupant breakout models predicted injury risk values well below the defined safety limits for dynamic loading certification (Table 3). These results indicate that the simulation predicts low injury risk in the ditching event. This finding is consistent with the Hudson River ditching event from which the impact conditions are taken. During the Hudson River ditching, there were five serious injuries that potentially occurred during the impact. None of these injuries were reported to be to the head, neck, or spine of the occupants [4]. Overall the occupant models predicted the highest risk of injury in the cervical spine region, with Nij values within 45% of the defined limit. Skull injury risk was predicted to be very low across the evaluated occupant positions with the highest HIC value at 11% of the certification limit.

Table 3. Computed Injury Metric Responses

Seat : ATD	Injury Metric Response			
	<u>HIC 15</u> (1000)	<u>HIC 36</u> (1000)	<u>Nij</u> (1)	<u>Lumbar</u> <u>Load</u> (1500)
Seat 1A: FAA H3 50th	7.7	15.8	0.14	398
Seat 3A: FAA H3 50th	104.2	104.2	0.32	122
Seat 3D: FAA H3 50th	107.7	107.7	0.3	128
Seat 3E: THOR	5.5	10.7	0.15	360
Seat 5A: H3 95th	48.8	56.2	0.38	381
Seat 5B: H3 5th	15.4	23.1	0.4	174
Seat 6A: FAA H3 50th	105.4	105.4	0.35	236
Seat 6B: FAA H3 50th*	2.5	3.5	0.22	50
Seat 6D: FAA H3 50th	72.9	72.9	0.45	210
Seat 9D: FAA H3 50th	5.9	3.2	0.07	311
Seat 10C: FAA H3 50th	29.2	31.1	0.15	150
Seat 12A: FAA H3 50th	68.3	68.3	0.23	250

*Braced position

The majority of occupant breakout models were simulated in the front section of the aircraft. This location was consistent with the conditions tested in the ground impact testing of the F28 aircraft. In the front section of the aircraft, Nij was the dominant injury driver for the majority of simulated occupants, with Nij responses showing a slightly increasing trend toward the rear of the front section (see Figure 25). There are two outliers in which lumbar load exhibits the dominant injury risk. The FAA H3 50th in seat 1A and the THOR ATD in seat 3E. Seat 1A faced a bulkhead with no forward seatback, which meant that all neck loads were due to inertial force, resulting in decreased loading of the neck compared to the ATD's which experienced seatback contact. The THOR in seat 3E also did not experience seatback contact due to differences in its kinematic response compared to the FAA H3 50th, which was seated in the adjacent seat 3D. The FAA H3 50th in seat 6D, which was in the braced posture, also predicted significantly different injury responses compared to the upright FAA H3 50th positioned adjacent.



*Braced position

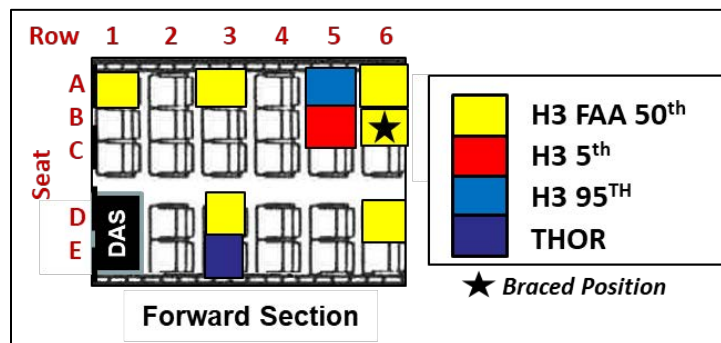


Figure 25. Normalized injury metric responses predicted in the front section of the aircraft (top) and reference schematic of ATD positioning (bottom).

Detailed comparisons of the FAA H3 50th in seat 3D and the THOR in seat 3E show differences in kinematic response of the torso and neck between the two ATDs, which results in a difference in prediction of head contact for a 50th percentile occupant made between the different ATD configurations. The H3 FAA 50th ATD was found to bend at the lumbar spine, the only flexible component of the H3 thoracic-lumbar spinal column, resulting in significant forward flexion of the head and torso. The THOR ATD exhibited more of a curling response, with significant flexion in the cervical spine and minimal flexion within the thoracic-lumbar region in the upper and lower flex joints (see Figure 26). The difference in spinal flexibility of the THOR ATD prevented contact with the forward seatback, which is a significant change in its interaction with the environment and altered the predicted risk of injury for a 50th percentile occupant between these two ATD configurations.

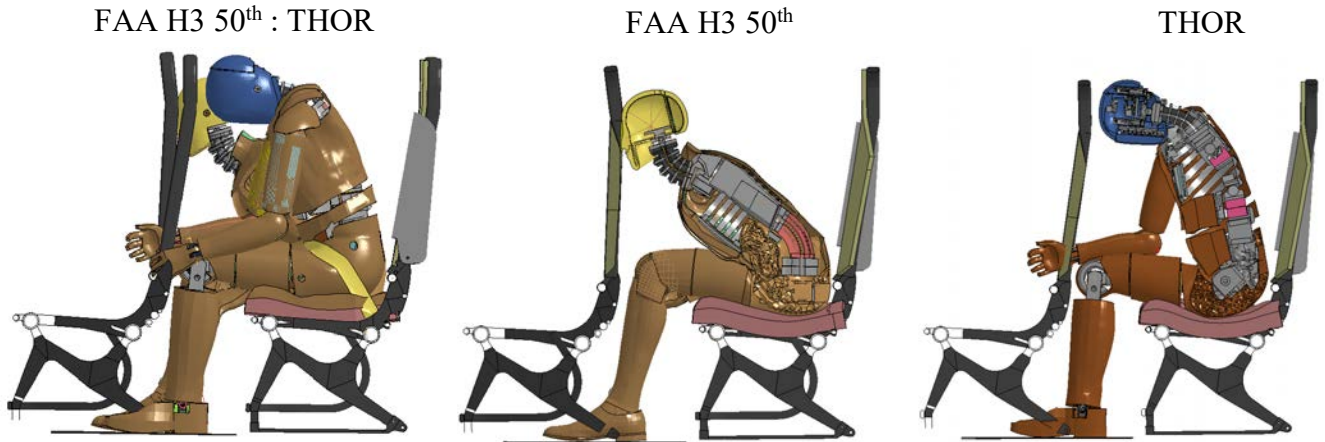


Figure 26. Row 3 Starboard ATD kinematic response at completion of simulation: FAA H3 50th versus THOR.

The braced FAA H3 50th ATD seated in seat 6B predicted lower HIC, Nij, and lumbar load values than the upright FAA H3 50th in the adjacent seat 6A. As the head of the braced ATD was closer to the forward seatback, contact occurred earlier during the impact event. This contact resulted in a smaller differential between head and seat velocity, less time for the ATD to accelerate with respect to the seat prior to contact, and thus a lower transfer of force into the head-neck region of the braced ATD on contact. This effect can be seen in the kinematic response of two ATDs (see Figure 27), with the braced ATD exhibiting reduced neck flexion during head-to-seat contact than the nominally positioned ATD.

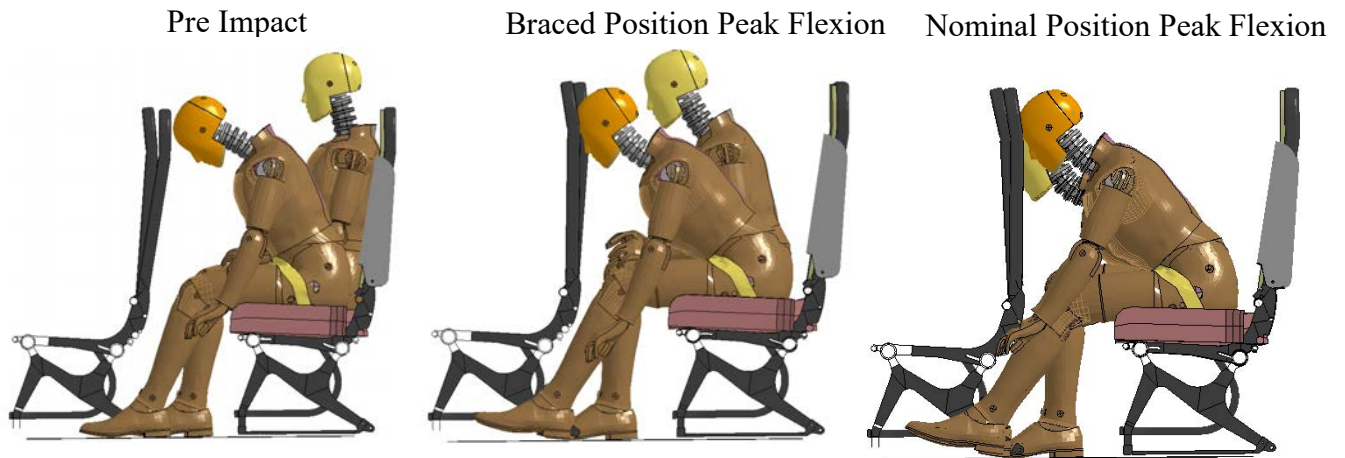


Figure 27. Row 6 Port ATD kinematics: braced versus nominal position

It should be noted that two of the injuries occurring in the Flight 1549 Hudson River ditching event were associated with occupants taking the braced position. These injuries were to the shoulders of the occupant [4]. The lower injury risk values demonstrated by the ATD in a braced position within this study apply only to skull and vertebral injuries and should not be extended to any determination of full body injury risk.

The H3 5th ATD predicts the second highest injury risk in the front section of the aircraft. The Nij value predicted by the H3 5th ATD is higher than the H3 95th ATD seated adjacent. In this condition Nij values calculated are primarily driven by compression of the neck as the head impacts the forward seatback. Although the H3 95th measures a larger peak compressive force, namely due to the larger upper body mass behind the head contact, a higher Nij value is predicted for the H3 5th (see Figure 28). This finding is because the intercept values used to calculate Nij are lower for the 5th in order to account for higher susceptibility for injury under equal load for the smaller anthropometry. The calculated lumbar load risk is higher in the H3 95th than the H3 5th because a limit based on the 50th percentile occupant size is used for both ATDs, the FAA does not define limits for the other two ATD sizes. The larger H3 95th mass results in larger compressive forces on the lumbar spine. This calculation does not account for increased musculature and vertebral strength in the larger occupant which may offset the increased load. Application of anthropometry specific lumbar load limits such as those developed for military rotorcraft [35] may provide improved injury prediction across the 5th-95th anthropometric range in general aviation safety analysis.

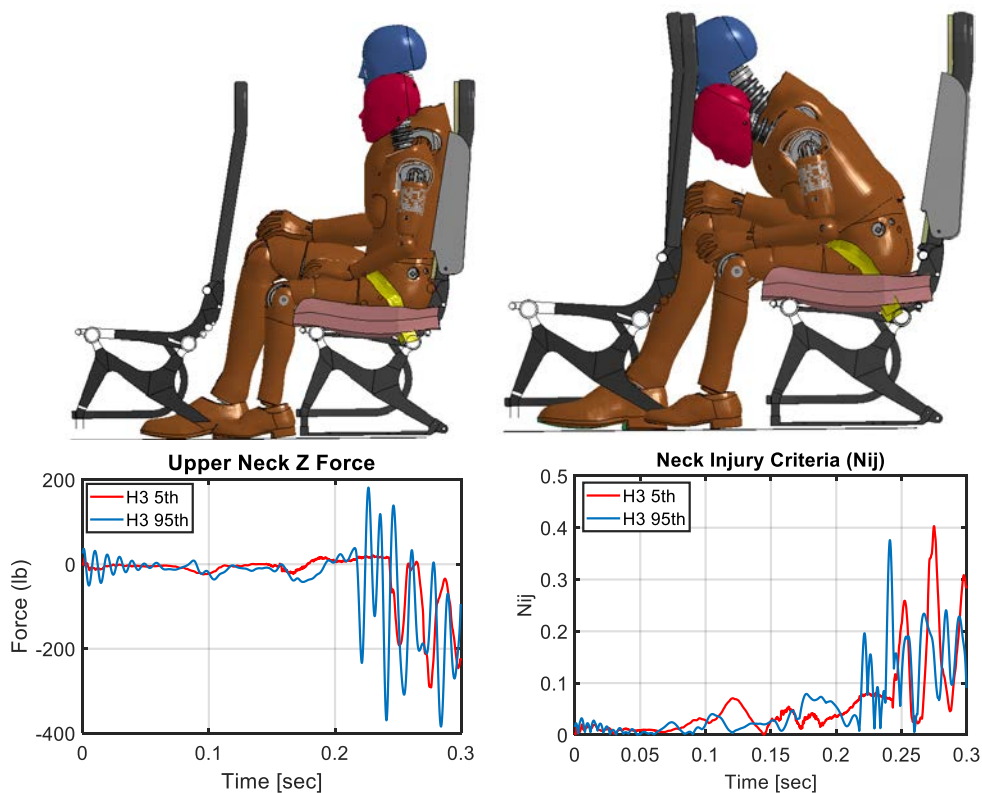


Figure 28. Row 5 Port side ATD kinematics (top) and upper neck response time history (bottom): H3 5th versus H3 95th.

A single occupant simulation was performed over the wing-box of the aircraft. Seat 9D was evaluated as a representative exit row configuration. With no forward seatback, lumbar load was shown to dominate injury risk predictions (see Figure 29). Predicted landing loads were not

significant enough to induce head-to-leg contact thus HIC values were negligible and inertial neck loading produced minimal Nij response. Lumbar load values were slightly higher than those observed towards the rear of the forward section.

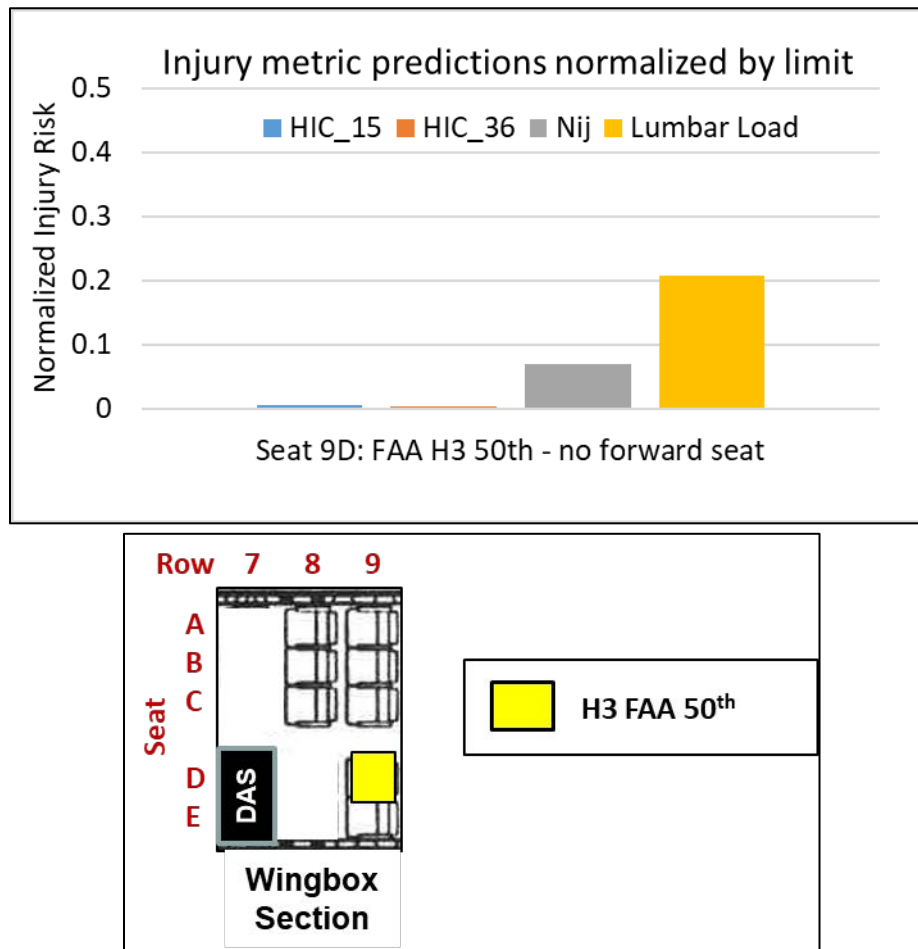


Figure 29. Normalized injury metric responses predicted in the wing-box section of the aircraft (top) and reference schematic of ATD positioning (bottom).

Occupant injury risk predicted in the aft section of the aircraft exhibited similar distribution of risk regions to those in standard seating configurations throughout the aircraft (see Figure 30). The FAA H3 50th in seat 10C exhibited the lowest overall injury risk with respect to all other occupant models simulated. These results are consistent with results observed in previous crash testing and simulation of this seating configuration [17, 22]. ATDs seated in seat 'C' which is overhanging, i.e. it does not have direct floor support below the seat, have exhibited reduced loading during the crash event compared to those in other seating positions. The lack of support below seat C allows increased deformation over the inner two seats, which causes it to absorb a larger portion of the crash energy and reduce loads transferred to the occupant.

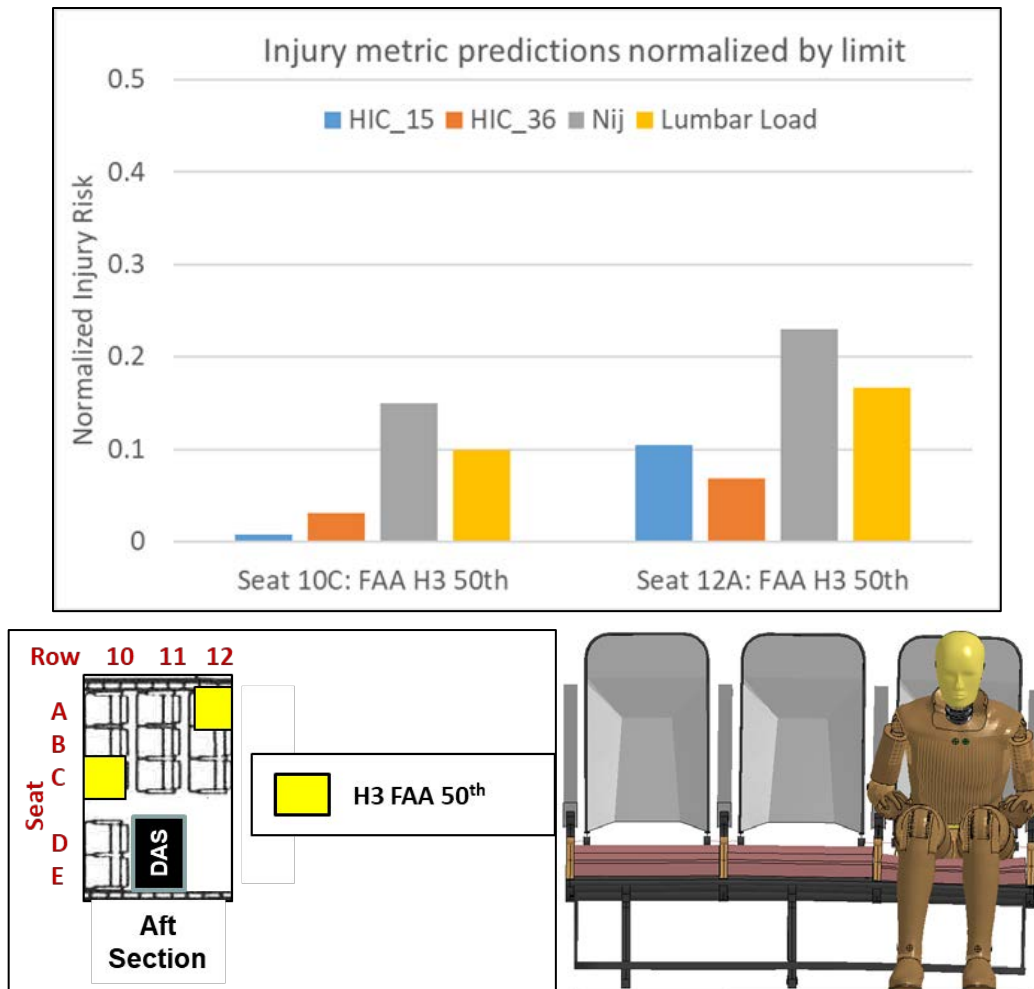


Figure 30. Normalized injury metric responses predicted in the Aft section of the aircraft (top), reference schematic of ATD positioning (bottom-left), and seat support deformation observed in simulation of seat 10C (bottom-right).

5. DISCUSSION OF RESULTS

A previously validated finite element model of a Fokker F28 Fellowship aircraft was analyzed for the water impact conditions of US Airways Flight 1549 ditching into the Hudson River in January 2009. The LS-DYNA[®] simulation was executed for impact conditions that were determined by the NTSB to be: V_x (forward velocity) = 211 ft/s (2,532 in/s) and V_z (vertical velocity) = 12.5 ft/s (150 in/s). The impact attitude was: Roll = 0.0°, Pitch (nose-up) = 9.5°, and Yaw = 0.0°. This FSI simulation was executed using the ALE capability in LS-DYNA[®].

Results were presented in several categories: (1) A320 recovery and damage assessment, (2) F28 predicted structural (seat base and airframe) accelerations, (3) F28 predicted model kinematic responses, impact sequences and damage, and (4) F28 predicted occupant responses and injury risk assessment.

The forward seat base and airframe accelerations predicted for the F28 aircraft during the US Airways Flight 1549 ditching event are low, generally less than 15 g. The vertical accelerations are also low, generally less than 15 g as well. The low acceleration response predicted within the cabin of the F28 aircraft resulted in subsequently minimal loading of the occupant models evaluated. Overall injury risk prediction is low, with all injury metrics calculated falling below 50% of the defined limits. The neck injury risk metric, N_{ij} , exhibits the highest value with respect to injury limits, followed by lumbar load. HIC values are negligible throughout the occupant models evaluated. The increased spinal flexibility of the THOR ATD over the Hybrid III ATD is shown to result in a difference in injury metric predictions, as different kinematic response leads to a difference in interactions with the forward seatback during the impact event. The braced position is shown to result in reduced injury metric values compared to an upright posture as it reduces closing velocity with the forward seatback as well as changes the orientation of load into the lumbar spine. Of note, two passenger injuries recorded during the Flight 1549 ditching event were shoulder injuries associated with passengers taking the braced position. Although this study indicates reduced neck and spinal injury metrics in the braced position, a more detailed study of the full body response in the braced position would be required to make a determination on its effectiveness in reducing total injury risk during a ditching event. The lack of head, neck, and spinal injury predicted by the F28 occupant models is consistent with the fact that no injuries in these body regions were reported in the Flight 1549 ditching event. This qualitative agreement between the F28 predicted occupant injury risk and the Flight 1549 injury report provides increased confidence in the use of these tools in predicting occupant injury risk during future ditching events.

One feature of the simulation that requires additional explanation is the long runtime. To execute an end time of 1.0 s, the model required 1,902 hours or 79.25 days. This excessive runtime is attributed to the 'nadv' parameter on the *CONTROL_ALE card, which controls how often the mesh is advected. Originally the model was simulated with the nadv parameter set to 5, which reduced simulation runtime to 424 hours or 18 days but resulted in significant mesh distortion (see Figure 31). The LS-DYNA User's Manual [5] recommends that the parameter be set to 1.0, meaning that the mesh is advected every time step. To evaluate the tradeoff between computation time and mesh stability a sensitivity study was performed varying the parameter between 1 and 5. Although nadv=1 was extremely computationally expensive, it was selected for displaying final results as it was the only value to completely remove the mesh distortion effects observed at the higher nadv values.

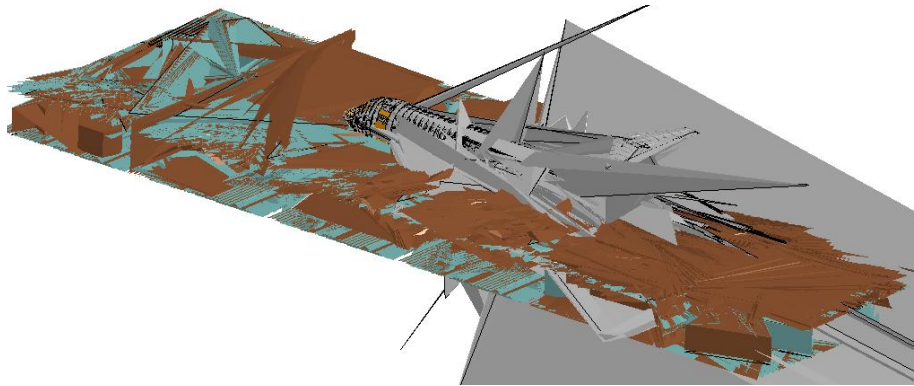


Figure 31. Mesh distortion.

6. CONCLUSIONS

A previously validated finite element model of a Fokker F28 Fellowship aircraft was used to perform LS-DYNA® simulations for water ditching conditions consistent with US Airways Flight 1549 crash into the Hudson River. The F28 model was simulated for the Flight 1549 impact conditions in order to evaluate its ability to predict structural and occupant responses in a realistic water ditching environment. Impact conditions recorded from the Flight 1549 event were used to drive a Fluid-Structure Interaction simulation of the event using the Arbitrary Lagrangian-Eulerian (ALE) capability within LS-DYNA®. Several categories of predicted vehicle structural responses were evaluated: impact kinematics (velocity time histories and impact sequences), seat and airframe acceleration responses, and airframe damage. In addition, occupant breakout models were developed and simulated using the seat base accelerations predicted by the F28 vehicle model. These occupant breakout models were used to predict occupant injury risk across a variety of seat locations, occupant positions, and Anthropomorphic Test Device types.

The simulation predicted seat base and airframe accelerations in both the vertical and forward directions to be low, less than 15 g, resulting in a fairly benign impact event. Likewise, simulations of the occupant breakout models predicted head, neck, and spinal injury metric values well below the defined safety limits for dynamic loading certification. These results were consistent with the lack of head, neck, or spinal injuries recorded in the ditching event. The LS-DYNA® simulation predicted damage to the lower rear portion of the airframe, as a result of the 9.5° pitch nose-up initial impact. Although it is difficult to differentiate damage caused by the water impact from that caused by retrieval of the Flight 1549 aircraft, the damage predicted by the simulation is similar to that seen on the Flight 1549 aircraft post-recovery. These results indicate reasonable prediction of a ditching event by the F28 model using ALE capability within LS-DYNA® and lend confidence for future use of water impact simulation.

7. REFERENCES

1. Credeur M. J., and Schlangenstein M., "US Airways Pilot Averts Tragedy in 'Miracle' Landing," www.Bloomberg.com, New York, January 16, 2009.
2. Patel, A. A., and Greenwood, R. P., "Transport Water Impact and Ditching Performance," DOT/FAA/AR-95/54, March 1996.
3. Fisher L. J., and Hoffman E. L., "Ditching Investigations of Dynamic Models and Effects of Design Parameters on Ditching Characteristics," NACA Technical Note 1347, 1957.
4. National Transportation Safety Board (NTSB) Report, "Loss of Thrust in Both Engines After Encountering a Flock of Birds and Subsequent Ditching on the Hudson River US Airways Flight 1549 Airbus A320-214, AAR-10/03, January 2009.
5. Hallquist J. Q., "LS-DYNA® Keyword User's Manual," Version 971, Livermore Software Technology Company, Livermore, CA, August 2006.
6. Fasanella E. L., Jackson K. E., Sparks C. E., and Sareen A. K., "Water Impact Test and Simulation of a Composite Energy Absorbing Fuselage Section," *Journal of the American Helicopter Society*, Vol. 50, No. 2, April 2005, pp. 150-164.
7. Jackson K. E., and Fuchs Y. T., "Comparison of ALE and SPH Simulations of Vertical Drop Tests of a Composite Fuselage Section into Water," Proceedings of the 10th International LS-DYNA® Users Conference, Dearborn, MI, June 8-10, 2008.
8. Vassilakos G. J., "Elemental Water Impact Test: Phase 1 20-inch Hemisphere," NASA/CR-2015-218679, January 2015.
9. Fasanella E. L., Jackson K. E., Lyle K. H., Sparks C. E., and Sareen A., "Multi-Terrain Impact Testing and Simulation of a Composite Energy Absorbing Fuselage Section," Proceedings of the American Helicopter Society Forum 60, Baltimore, MD, June 8-10, 2004.
10. Vassilakos G. J., and Mark S. D. "Boilerplate Test Article (BTA) Water Impact Test Correlation," NASA Contractor Report, NASA/CR-2017-219792, November 2017.
11. Jones L. E., "Overview of the NASA Systems Approach to Crashworthiness Program," Proceedings of the American Helicopter Society 58th Annual Forum, Montreal Canada, June 11-13, 2002.
12. *Federal Register*. Federal Aviation Administration, Aviation Rulemaking Advisory Committee, Transport Airplane and Engine Issues, Vol 80. 2015.
13. Jackson K. E., Littell J. D., Annett M. S. and Haskin I. M., "Vertical Drop Test and Simulation of a Fokker F-28 Fuselage Section," Proceedings of the ASCE 2018 Earth and Space Conference, Cleveland, OH, April 11-13, 2018.
14. Jackson K. E., Littell J. D., Annett M. S. and Haskin I. M., "Finite Element Simulations of Two Vertical Drop Tests of F-28 Fuselage Sections," NASA Technical Memorandum NASA/TM-2018-219807, February 2018.

15. Littell J. D. "Full Scale Drop Test of a Fokker F28 Forward Fuselage Section onto Soil," Proceedings of the Aerospace Structural Impact Dynamics International Conference, Wichita, KS, October 17-19, 2017.
16. Littell J. D. "Full-Scale Drop Test of a Fokker F28 Wing-Box Fuselage Section," Proceedings of the 16th Biennial ASCE Earth and Space Conference, Cleveland, OH, April 9-12, 2018.
17. Littell J. D., "A Summary of Results from Two Full-Scale Fokker F28 Fuselage Section Drop Tests," NASA/TM-2018-219829, May 2018.
18. Vaughan V. L. Jr. and Alfaro-Bou E., "Impact Dynamics Research Facility for Full-Scale Aircraft Crash Testing," NASA TN D-8179, 1976.
19. Littell J. D., "A Summary of Airframe Results from a Fokker F-28 Full-Scale Crash Test," NASA Technical Memorandum, NASA/TM-2020-220572, March 2020.
20. Anon. "MSC/NASTRAN Quick Reference Guide," Version 70.5, The MacNeal-Schwendler Corporation, Los Angeles, CA, February 1998.
21. Jackson K. E. and Putnam J. B. "Simulation of a Full-Scale Crash Test of a Fokker F28 Fellowship Aircraft," NASA Technical Memorandum NASA/TM-2020-220435, January 2020.
22. Putnam J. B. "Occupant Response Analysis of a Full-Scale Crash Test of a Fokker F28 Fellowship Aircraft," NASA Technical Memorandum NASA/TM-2020-220571, March 2020.
23. International Standards Organization (ISO) Technical Report, "Road vehicles - Objective rating metrics for dynamic systems," ISO/TR 16250, July 15, 2013.
24. Benson D. J., "Momentum Advection on a Staggered Mesh," *Journal of Computational Physics*, 109: 143-162, 1992.
25. Humanetics, "User's Manual FAA Hybrid III 50th Male Dummy LS-DYNA® Model Version 1.2.3," Humanetics Innovative Solutions, Plymouth, MI, 2018.
26. Humanetics, "Hybrid III 5th Percentile Female Dummy LS-DYNA® Model Version 7.0.5 User Manual." Humanetics Innovative Solutions, Plymouth, MI, 2013.
27. Guha S., "README LSTC H3_95TH_DETAILED Scaled. 151214.V3.03_BETA," Livermore Software Technology Corporation, MI, 2015.
28. Panzer M. B., et al., "THOR 50th Male Finite Element Model User Manual," Model Version 2.1 for LS-Dyna," 2015.
29. Putnam J. B., et al., "Development, calibration, and validation of a head-neck complex of THOR mod kit finite element model," *Traffic Injury Prevention* 15(8): 844-854, 2014.
30. Putnam J. B., et al., "Development and evaluation of a finite element model of the THOR for occupant protection of spaceflight crewmembers," *Accident Analysis & Prevention*, 82: 244-256, 2015.
31. LSTC, "LS-DYNA® Theory Manual," Livermore Software Technology Company, Livermore, CA, 2017.

32. Federal Aviation Administration, "14 CFR Part 25.562 Emergency landing dynamic conditions," Federal Aviation Regulation. Volume 53, Amdt. 25-64, 1988.
33. Kleinberger M., Sun E., Eppinger R., Kuppa S., and Saul R., "Development of Improved Injury Criteria for the Assessment of Advanced Automotive Restraint Systems," National Highway Traffic Safety Administration, Washington, DC, 1998.
34. National Highway Traffic Safety Administration, "Docket No. NHTSA-2015-0119." New Car Assessment Program (NCAP).
35. Bolukbasi A., Crocco J., Clarke C., Fasanella E., Jackson K., Keary P., et al., "Full Spectrum Crashworthiness Criteria for Rotorcraft," U.S. Army Research, Development and Engineering Command, Ft. Eustis, VA RDECOM TR 12-D-12, 2011.

REPORT DOCUMENTATION PAGE

Form Approved
OMB No. 0704-0188

The public reporting burden for this collection of information is estimated to average 1 hour per response, including the time for reviewing instructions, searching existing data sources, gathering and maintaining the data needed, and completing and reviewing the collection of information. Send comments regarding this burden estimate or any other aspect of this collection of information, including suggestions for reducing the burden, to Department of Defense, Washington Headquarters Services, Directorate for Information Operations and Reports (0704-0188), 1215 Jefferson Davis Highway, Suite 1204, Arlington, VA 22202-4302. Respondents should be aware that notwithstanding any other provision of law, no person shall be subject to any penalty for failing to comply with a collection of information if it does not display a currently valid OMB control number.
PLEASE DO NOT RETURN YOUR FORM TO THE ABOVE ADDRESS.

1. REPORT DATE (DD-MM-YYYY) 01/09/2020	2. REPORT TYPE TECHNICAL MEMORANDUM	3. DATES COVERED (From - To) 1-31-20 to 8-31-20
--	---	---

4. TITLE AND SUBTITLE LS-DYNA Water Ditching Simulation of a Fokker F28 Fellowship Aircraft	5a. CONTRACT NUMBER
	5b. GRANT NUMBER
	5c. PROGRAM ELEMENT NUMBER

6. AUTHOR(S) Karen E. Jackson Jacob B. Putnam	5d. PROJECT NUMBER
	5e. TASK NUMBER
	5f. WORK UNIT NUMBER 031102.02.07.16.9DA2.19

7. PERFORMING ORGANIZATION NAME(S) AND ADDRESS(ES) NASA Langley Research Center Hampton, VA 23681-2199	8. PERFORMING ORGANIZATION REPORT NUMBER
---	---

9. SPONSORING/MONITORING AGENCY NAME(S) AND ADDRESS(ES) National Aeronautics and Space Administration Washington, DC 20546-001	10. SPONSOR/MONITOR'S ACRONYM(S) NASA
	11. SPONSOR/MONITOR'S REPORT NUMBER(S) NASA/TM-2020-5006941

12. DISTRIBUTION/AVAILABILITY STATEMENT
Unclassified - Unlimited
Subject Category
Availability: NASA STI Program (757) 864-9658

13. SUPPLEMENTARY NOTES
This work was sponsored by the FAA William J. Hughes Technical Center.

14. ABSTRACT
A previously validated finite element model of a Fokker F28 Fellowship aircraft was used to perform LS-DYNA simulations for water ditching conditions consistent with US Airways Flight 1549 crash into the Hudson River. The LS-DYNA model of the F28 was originally developed from an existing NASTRAN loads model and was validated through test-analysis comparisons with data from a full-scale crash test of the F28 onto soil. The F28 aircraft was simulated for the Flight 1549 impact conditions, not to precisely predict the response of the Airbus A320 aircraft used for that flight, but to evaluate tools for simulating and analyzing water impacts using a realistic aircraft ditching event. Flight 1549 impact conditions were: Vx (f

15. SUBJECT TERMS
simulating transport aircraft ditching, LS-DYNA, Arbitrary Lagrangian-Eulerian (ALE), occupant modeling and injury risk prediction

16. SECURITY CLASSIFICATION OF:			17. LIMITATION OF ABSTRACT UU	18. NUMBER OF PAGES 47	19a. NAME OF RESPONSIBLE PERSON HQ - STI-infodesk@mail.nasa.gov
a. REPORT U	b. ABSTRACT U	c. THIS PAGE U			19b. TELEPHONE NUMBER (Include area code) 757-864-9658